

DOT/FAA/AR-08/37,P3

Air Traffic Organization
Operations Planning
Office of Aviation Research
and Development
Washington, DC 20591

Explicit Finite Element Modeling of Multilayer Composite Fabric for Gas Turbine Engine Containment Systems, Phase II

Part 3: Material Model Development and Simulation of Experiments

February 2009

Final Report

This document is available to the U.S. public through
the National Technical Information Service (NTIS),
Springfield, Virginia 22161.



U.S. Department of Transportation
Federal Aviation Administration

NOTICE

This document is disseminated under the sponsorship of the U.S. Department of Transportation in the interest of information exchange. The United States Government assumes no liability for the contents or use thereof. The United States Government does not endorse products or manufacturers. Trade or manufacturer's names appear herein solely because they are considered essential to the objective of this report. This document does not constitute FAA certification policy. Consult your local FAA aircraft certification office as to its use.

This report is available at the Federal Aviation Administration William J. Hughes Technical Center's Full-Text Technical Reports page: actlibrary.tc.faa.gov in Adobe Acrobat portable document format (PDF).

1. Report No. DOT/FAA/AR-08/37,P3		2. Government Accession No.		3. Recipient's Catalog No.	
4. Title and Subtitle EXPLICIT FINITE ELEMENT MODELING OF MULTILAYER COMPOSITE FABRIC FOR GAS TURBINE ENGINE CONTAINMENT SYSTEMS, PHASE II, PART 3: MATERIAL MODEL DEVELOPMENT AND SIMULATION OF EXPERIMENTS				5. Report Date February 2009	
				6. Performing Organization Code	
7. Author(s) Jeffrey Simons, David Erlich, and Donald Shockey				8. Performing Organization Report No.	
9. Performing Organization Name and Address SRI International 333 Ravenswood Avenue Menlo Park, CA 94025				10. Work Unit No. (TRAVIS)	
				11. Contract or Grant No.	
12. Sponsoring Agency Name and Address U.S. Department of Transportation Federal Aviation Administration Air Traffic Organization Operations Planning Office of Aviation Research and Development Washington, DC 20591				13. Type of Report and Period Covered Final Report	
				14. Sponsoring Agency Code ANM-100/AME-100	
15. Supplementary Notes The Federal Aviation Administration Airport and Aircraft Safety R&D Division COTR was Don Altobelli.					
16. Abstract A team consisting of Arizona State University, Honeywell Engines, Systems & Services, the National Aeronautics and Space Administration Glenn Research Center, and SRI International collaborated to develop computational models and verification testing for designing and evaluating turbine engine fan blade fabric containment structures. This research was conducted under the Federal Aviation Administration Airworthiness Assurance Center of Excellence and was sponsored by the Aircraft Catastrophic Failure Prevention Program. The research was directed toward improving the modeling of a turbine engine fabric containment structure for an engine blade-out containment demonstration test required for certification of aircraft engines. The research conducted in Phase II began a new level of capability to design and develop fan blade containment systems for turbine engines. Significant progress was made in three areas: (1) further development of the ballistic fabric model to increase confidence and robustness in the material models for the Kevlar [®] and Zylon [®] material models developed in Phase I, (2) the capability was improved for finite element modeling of multiple layers of fabric using multiple layers of shell elements, and (3) large-scale simulations were performed. This report concentrates on the material model development and simulations of the impact tests.					
17. Key Words Finite element model, Fabric, Aircraft engine fragments, Fragment barriers, Kevlar			18. Distribution Statement This document is available to the U.S. public through the National Technical Information Service (NTIS), Springfield, Virginia 22161.		
19. Security Classif. (of this report) Unclassified		20. Security Classif. (of this page) Unclassified		21. No. of Pages 69	22. Price

TABLE OF CONTENTS

	Page
EXECUTIVE SUMMARY	xi
1. INTRODUCTION	1
1.1 PURPOSE	1
1.2 BACKGROUND	1
2. DISCUSSION	2
2.1 Material Model Versions	2
2.1.1 Fabric Model Version 1.0	3
2.1.2 Fabric Model Version 2	9
2.1.3 Fabric Model Version 3	9
2.1.4 Comparison of Version 3.1 to Version 1.0	13
2.2 LS-DYNA MODEL Versions	14
3. TASK 1: ROBUST FE MODEL DEVELOPMENT	14
3.1 Sensitivity Study of Model Performance (Task 1.1)	14
3.1.1 Test Configuration	14
3.1.2 The FE Model	16
3.1.3 Parameter Variations	16
3.1.4 Baseline	17
3.1.5 Measured Parameters (Task 1.1.1)	18
3.1.6 Estimated Parameters (Task 1.1.2)	20
3.1.7 Strain Rate Dependence of Failure (Task 1.1.3)	21
3.1.8 Numerical Considerations (Task 1.1.4)	22
3.1.9 Failure Parameters	27
3.1.10 Friction	31
3.1.11 Summary	31
3.2 Tension Testing (Task 1.3)	32
3.2.1 Simple Tension Testing (Task 1.3.1)	32
3.2.2 Tensile Tests Over a Range of Strain Rates (Task 1.3.2)	33
3.2.3 Zylon Strain Dependence Rate Tests	35
3.2.4 Kevlar Strain Rate Dependence Tests	36
3.2.5 Combined Strain Rate Test Results	37

3.3	Static Ring Test-to-FE Results Comparison (Task 1.6)	37
3.3.1	Simulation of 0° Ring Test With Constants From Static Uniaxial Test	38
3.3.2	Adjustment to Failure Strength Based on Ring Test Results	38
3.3.3	Results of Ring Tests With Increased Strength	40
3.4	Initial FE Simulations of NASA-GRC Ballistic Tests (Task 1.9)	41
3.4.1	Initial NASA-GRC Kevlar Simulations	41
3.4.2	Initial NASA-GRC Zylon Simulations	43
3.5	Material Model and Methods Update (Task 1.10)	45
3.5.1	Version 3.1-K3B Comparison With NASA-GRC Ballistic Tests	45
4.	TASK 2: IMPROVE FE MODELING CAPABILITY FOR MULTIPLE LAYERS OF FABRIC	47
4.1	Review Damage in Partially Penetrated Fabrics (Task 2.1.1)	47
4.2	Review Problem With Livermore Software Technology Corporation (Task 2.2)	49
4.3	Material Model and Methods Update (Task 2.4)	49
4.4	Demonstrate Results: Multiple Shell Layer Simulations for NASA-GRC Kevlar Tests (Task 2.3)	52
5.	CONCLUSIONS AND RECOMMENDATIONS	55
5.1	Conclusions	55
5.2	Recommendations	56
6.	REFERENCES	57

LIST OF FIGURES

Figure		Page
1	Uniaxial Stress-Strain Curve for Ballistic Fabric Model	4
2	Damage Function for Version 1.0 for Kevlar	5
3	Test Results and Fabric Model for Phase I Uniaxial Tests	5
4	Stress-Strain Curves for Different Rates Version 2	8
5	Rate Effect Model and Test	8
6	Version 3 Model Parameters	10
7	Version 3 Model Damage	11
8	Rate Effect Theory Version 3	12
9	Comparison of Version 1.0 and Version 3.1 Simulations of Phase I NASA-GRC Tests	14
10	The NASA-GRC Test Configuration	15
11	The FE Model of Impactor, Fabric, and Ring	15
12	Baseline Case	17
13	Effect of Crimp	18
14	Effect of Variations in Tensile Modulus	19
15	Effect of Variations in Unloading Modulus	20
16	Effect of Variations in Shear Modulus	21
17	Element Strain Rate History	22
18	Mesh Resolution Simulations	23
19	Effect of Variations in Element Type	24
20	Effect of Variations in Time Step	25
21	Effect of Variations in Slideline Parameter Soft	26
22	Effect of Variations in Number of Plies	27

23	Effect of Failure Strain on Energy Absorbed	28
24	Effect of Time Constant on Energy Absorbed	29
25	Stress-Strain Curves for Cases 26 and 27	30
26	Effect of Material Strength on Energy Absorbed	30
27	Effect of Friction	31
28	Uniaxial Tension Tests at ASU for Phase II and Version 3.1 Model Fit	33
29	University of Washington Applied Biomechanics Laboratory	33
30	High-Rate Tensile Test Schematic	34
31	High-Rate Test Grips	34
32	Failed Specimen	35
33	Variable-Rate Zylon Tensile Test Results	36
34	Variable-Rate Kevlar Tensile Test Results	36
35	Rate Test Strength Summary	37
36	Simulation of 4-Ply Kevlar Ring Test With Constants K3A	38
37	Ring Test Simulations Without Allowing Failure	39
38	Failure Surface for Kevlar Fabric Based on Ring Test Results	40
39	Kevlar Ring Test Simulation Results With Material Constant Set K3B	41
40	Version 3.1-K3A Simulations of NASA-GRC Kevlar Ballistic Tests	42
41	Energy Absorbed for Kevlar Tests Version 3.1-K3A	43
42	Version 3.1-Z3A Simulations of NASA-GRC Zylon Ballistic Tests	44
43	Comparison of Energy Absorbed for Zylon Model Version 3.1-Z3A	45
44	The NASA-GRC Ballistic Test Simulation Results for Kevlar for Version 3.1-K3B	46
45	Percentage KE Absorbed for NASA-GRC Kevlar Test for Version 3.1-K3B	47
46	Ply Damage for Test LG414	48
47	Effect of Modeling With Multiple Layers	51

48	Kinetic Energy for Multilayer Simulations	52
49	Kinetic Energy in Kevlar NASA-GRC Tests for Version 3.1-K3B Single and Multiple Shell Simulations	54
50	Energy Absorbed in NASA-GRC Kevlar Tests for Version 3.1 Multiple Layer Simulations	54
51	Difference in Absorbed KE for Single and Multiple Layer Simulations	55

LIST OF TABLES

Table		Page
1	Fabric Model Versions	2
2	Material Constants Versions	3
3	Physical Properties of Zylon and Kevlar Fabrics	6
4	Material Constants for Kevlar (K1A) and Zylon (Z1A)	6
5	Kevlar Material Constant Set K3A	12
6	Zylon Material Constant Set Z3A	13
7	Kevlar Material Constant Set K3B	13
8	Parameter Variations for No-Damage Simulations	16
9	Parameter Study for Failure Parameters	27
10	The NASA-GRC Ballistic Tests on Kevlar Targets With Model Version 3.1-K3A	42
11	The NASA-GRC Ballistic Tests on Zylon Targets With Model Version 3.1-Z3A	44
12	The NASA-GRC Test Simulation Results for Kevlar Version 3.1-K3B	46
13	Contact Parameters for Multilayer Shells	50
14	Results of Multiple Shell Simulations of LG646 and LG647	51
15	Multiple Shell Layer Results Version 3.1-K3B	53

LIST OF SYMBOLS AND ACRONYMS

ϵ_{80}	Strain at 80% of peak stress
ϵ_{crx}	Crimp strain in x direction
ϵ_{cry}	Crimp strain in y direction
ϵ_{max}	Strain at maximum stress
ϵ_{min}	Strain at initial damage
σ_{max}	Maximum stress
cr	Crimp modulus normalized by tensile modulus
co	Compression modulus normalized by tensile modulus
E	Tensile modulus
E_b	Baseline tensile modulus = 13.3 Msi
$2G$	Shear modulus
m	Damage rate exponent for Version 3 damage function
n	Exponent for driving stress in Version 3 damage function
t_c	Time constant for rate effects
unl	Unloading modulus normalized by tensile modulus
ASU	Arizona State University
D	Denier
FAA	Federal Aviation Administration
FE	Finite element
GWU	George Washington University
KE	Kinetic energy
Msi	Million pounds per square inch
NASA-GRC	National Aeronautics and Space Administration Glenn Research Center
SRI	SRI International
UW	University of Washington
LSTC	Livermore Software Technology Corporation

EXECUTIVE SUMMARY

A team consisting of Arizona State University (ASU), Honeywell Engines, Systems & Services, the National Aeronautics and Space Administration Glenn Research Center (NASA-GRC), and SRI International (SRI) collaborated to develop computational models and verification testing for designing and evaluating turbine engine fan blade fabric containment structures. This research was conducted under the Federal Aviation Administration Airworthiness Assurance Center of Excellence and sponsored by the Aircraft Catastrophic Failure Prevention Program. The research was directed toward improving the modeling of a turbine engine fabric containment structure for an engine blade-out containment demonstration test required for certification of aircraft engines.

In Phase I, progress was made in testing and computational analysis. A material model was developed for Kevlar[®] and Zylon[®] fabrics. Static testing of containment wraps subjected to loads through a blunt-nose impactor was performed at ASU. Ballistic testing of containment wraps subjected to a high-velocity blunt projectile was performed at NASA-GRC. These tests have provided test cases (benchmark results) to validate the developed finite element (FE) methodology. While the work performed in Phase I met the stated objectives, improvements in robustness and confidence of the FE simulations and predictions were desired.

The research conducted in Phase II brought a new level of capability to design and develop fan blade containment systems for turbine engines. To achieve the program objectives, a plan consisting of the following four technical tasks was developed and implemented:

- Task 1: Robust FE Model Development. The objective of this task was to increase confidence and robustness in the material models for the Kevlar and Zylon material models developed in Phase I.
- Task 2: Improve FE Modeling Capability for Multiple Layers of Fabric. In Phase I, most LS-DYNA[®] models used a single-element through the thickness to model the fabric, ranging from 1 to 24 layers.
- Task 3: 1500 denier (D) Zylon Material Model Development. In Phase I, limited ballistic and static tests of 1500 D Zylon indicated this configuration of Zylon might have the potential to offer a 60% weight advantage over a similar configuration of Kevlar 49 fabric for the same fragment energy. The objective of this task was to develop and validate a material model for 1500 D Zylon. It should be noted that during this research, it was discovered that Zylon was found to have excessive deterioration due to heat and humidity. As a result, it was decided that the remainder of this research would focus only on Kevlar fabrics.
- Task 4: Engine Simulations. As in Phase I, the objective of this task was to validate improvements to the material models and FE methods developed under Phase II as they relate to propulsion engine fan blade containment. Existing fabric material models and modeling methods and their improvements were validated using fan containment test data.

Each member of the team developed a comprehensive report describing the details of the research task and the findings. The comprehensive report consists of the following four reports:

- ASU Department of Civil Engineering, Part 1: Fabric Material Tests
- NASA-GRC, Part 2: Ballistic Impact Testing
- SRI International, Part 3: Material Model Development and Simulation of Experiments
- Honeywell Engines, Systems & Services, Part 4: Model Simulation for Ballistic Tests, Engine Fan Blade-Out, and Generic Engine Model

SRI's effort in Phase II is presented in this report (Part 3). SRI's part was to (1) perform static laboratory experiments (swath tests) to measure response of multilayer fabrics to slow penetration, (2) use the data and observations along with ring test data from ASU and ballistic data from NASA-GRC to develop a computational model of fabric response, and (3) evaluate the model by simulating the experiments and comparing computed and observed behavior. The procedures and results of this effort are also presented.

1. INTRODUCTION.

1.1 PURPOSE.

The primary focus of this research was to address the technology gaps in containment events simulation and develop a robust modeling methodology for the analysis of a fan blade-out event in a multilayer fabric containment system. Specific program objectives are:

- Combine the LS-DYNA[®] modeling expertise of Honeywell Engines, Systems & Services (Honeywell), with the material modeling capability of SRI International (SRI), the ballistic testing capabilities of the National Aeronautics Space Administration Glenn Research Center (NASA-GRC), and the experimental facilities and finite element (FE) analysis/modeling capabilities of Arizona State University (ASU).
- Incorporate the material models, developed by SRI, into the LS-DYNA modeling methodology, developed by Honeywell, and correlate them to the results from controlled laboratory hardware tests, and then develop new methodologies if necessary.
- Develop methodologies for numerical simulation of engine fan blade-out events with fiber fabric wraps using SRI's material models and Honeywell's LS-DYNA modeling methodology. Validate the methodologies using existing engine fan blade-out containment test results from Honeywell.
- Compare the efficiency of Kevlar[®] and Zylon[®] wraps through laboratory hardware tests and LS-DYNA analysis of the test coupons.
- Explore the potential of 1500 denier (D) Zylon for future gas turbine engine containment systems.

During this study, the planned development of Zylon material models was suspended due to potential material strength degradation issues under environmental conditions. Funding was redirected toward completion of Tasks 1 and 2 with Kevlar material.

1.2 BACKGROUND.

A team consisting of ASU, Honeywell, NASA-GRC, and SRI personnel collaborated to develop computational models and verification tests for designing and evaluating turbine engine fan blade fabric containment structures. This research was conducted under the Federal Aviation Administration (FAA) Airworthiness Assurance Center of Excellence and sponsored by the Aircraft Catastrophic Failure Prevention Program. The research was directed toward improving the modeling of a turbine engine fabric containment structure for an engine blade-out containment demonstration test required for certification of aircraft engines.

In Phase I [1-4], progress was made in testing and computational analysis. A fabric material model was developed for Kevlar and Zylon fabrics. Static testing of containment wraps subjected to loads through a blunt-nose impactor was carried out at ASU. Ballistic tests of containment wraps subjected to a high-velocity blunt projectile were conducted at NASA-GRC.

These tests provide the test cases (benchmark results) to validate the developed finite element methodology. While the work performed in the previous research program met the stated objectives, improvements in robustness and confidence of the FE simulations and predictions was desired.

SRI's effort in the ASU/Honeywell/NASA-GRC program is presented here. The objective of the ASU/Honeywell/NASA-GRC program was to further develop and demonstrate a computational model of ballistic response of fabrics under engine containment conditions. The desired result was a computational capability for designing multilayer fabric engine containment structures for commercial transport aircraft. SRI's part was to (1) perform static laboratory experiments (swath tests) to measure response of multilayer fabrics to slow penetration, (2) use the data and observations with ring test data from ASU and ballistic data from NASA-GRC to develop a computational model of fabric response, and (3) evaluate the model by simulating the experiments and comparing computed and observed behavior. The procedures and results of this effort are presented in the following sections.

2. DISCUSSION.

2.1 MATERIAL MODEL VERSIONS.

The ballistic fabric model developed by SRI for this program is in Version 3.0, as listed in table 1. Version 1.0 was developed for Phase I of this program based on static uniaxial tests of Kevlar and Zylon and then used to simulate ballistics tests conducted at NASA-GRC. Version 2.0 contained incremental modifications, primarily a modified definition of how a fabric fails, namely that yarns in both directions must fail before the fabric can be penetrated. In Version 1.0, fabric failure occurred if yarns fully failed in either direction. A potential problem associated with calculation of a square root during unloading was removed for Version 2.1. Version 2.1 was available at the beginning of Phase II and was used in the parameter study described in section 3.1. Versions 3.0 and 3.1 were developed as a result of new data generated in Phase II at ASU and NASA-GRC with the projectiles oriented over a range of pitch, yaw, and roll values. Version 3.1 was used in the simulations of NASA-GRC ballistics tests for Phase II.

Table 1. Fabric Model Versions

Version	Date	Fundamental Changes	Usage
Version 1.0	2/12/2002		Phase I ballistic tests
Version 2.0	6/30/2004	Failure needs to break yarns in both directions	Phase II (did not run on some computers due to square root calculation)
Version 2.1	11/30/2004	Removed square root calculation in unloading	Phase II parameter study
Version 3.0	8/17/2005	1) Modified damage function 2) Modified rate dependence 3) Simplified version for unloading	Development of modified rate and damage functions
Version 3.1	5/31/2006	Full version for unloading	NASA-GRC Phase II ballistic tests

Different values for material constants were also developed based on the test data available and are listed in table 2. For Kevlar, three sets of material constants were used, and for Zylon, set Z1A was used for Versions 1.0 and 2.1 and Z3A for Versions 3.0 and 3.1. In subsequent discussions, the material models description for the simulations will include both the version number for the model and the material constants set; e.g., Version 3.1-K3A, means Version 3.1 of the model using material constants set K3A.

Table 2. Material Constants Versions

Version	Material	Based on
K1A	Kevlar 49	Phase I uniaxial data
K3A	Kevlar 49	Phase II uniaxial test data and rate data
K3B	Kevlar 49	Ring test with roll
Z1A	Zylon 500 D	Phase I uniaxial data
Z3A	Zylon 500 D	Phase II uniaxial test data and rate data

2.1.1 Fabric Model Version 1.0.

This description of Version 1.0 of the fabric model was taken from the Phase I final report [3]. The ballistic fabric model is orthotropic with stress-strain response, for each two yarn (local X and Y) directions, as shown in figure 1. The stress-strain responses in the two directions are uncoupled.

$$\begin{aligned}
 \sigma_{xx} &= f(\varepsilon_{xx}) \\
 \sigma_{yy} &= f(\varepsilon_{yy}) \\
 \sigma_{zz} &= 0 \\
 \tau_{xy} &= G\varepsilon_{xy} \\
 \tau_{yz} &= G\varepsilon_{yz} \\
 \tau_{zx} &= G\varepsilon_{zx}
 \end{aligned} \tag{1}$$

As shown in figure 1, the uniaxial response has the following features:

- Initial crimp before straightening, prestraightened modulus = $cr \cdot E$
- Linear response after straightening with modulus E up to a strain of first nonlinearity, ε_{min}
- Peak stress, σ_{max} , and strain at peak stress, ε_{max}
- Linear elastic unloading with modulus of $2E$ and with reduced modulus with damage
- Post peak softening characterized by softening strain measure, ε_{soft}
- Failure (element erosion) at full damage

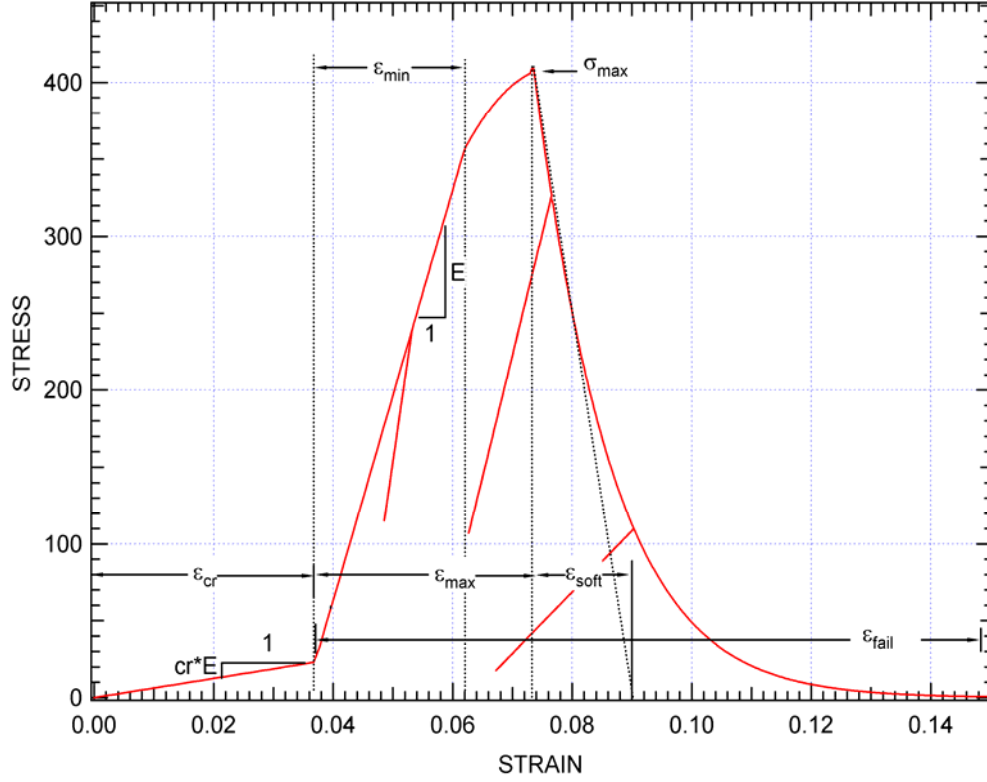


Figure 1. Uniaxial Stress-Strain Curve for Ballistic Fabric Model

2.1.1.1 Damage Function in Version 1.0.

In the ballistic fabric model, it was assumed that the individual fibers that make up the yarns have linear elastic response until they break, but that the fibers break at different values of overall strain. The fraction of broken fibers is called the damage function, d . The average stress for any value of strain is given by the stress in the fibers times the fraction of fibers that are unbroken.

The damage to the fabric as a function of strain can then be calculated by comparing the measured stress-strain curve to the elastic curve, assuming that no fibers break. For Version 1.0, the damage function, d , was defined in each direction as a function of the strain quantity, $\bar{\epsilon}$, in that direction and d_p was defined as the damage function at the peak stress as follows:

$$d = 0 \quad \text{where} \quad \bar{\epsilon} \leq \epsilon_{\min} + \epsilon_{cr} \quad (2a)$$

$$d = \frac{d_p (\bar{\epsilon} - \epsilon_{\min} - \epsilon_{cr})}{(\epsilon_{\max} - \epsilon_{\min})} \quad \text{where} \quad \epsilon_{\max} + \epsilon_{cr} \geq \bar{\epsilon} > \epsilon_{\min} + \epsilon_{cr} \quad (2b)$$

$$d = d_p \left(1 - \exp \left(- \frac{\bar{\epsilon} - (\epsilon_{\max} + \epsilon_{cr})}{\epsilon_{soft}} \right) \right) \quad \text{where} \quad \bar{\epsilon} > \epsilon_{\max} + \epsilon_{cr} \quad (2c)$$

The meaning of the various strain limits, ϵ_{cr} , ϵ_{min} , ϵ_{max} , and ϵ_{soft} are shown in figure 2. The calculation of $\bar{\epsilon}$ is discussed below. This piece-wise damage function results in a sharp peak for the stress-strain curve, which was characteristic of the uniaxial stress-strain curves for the fabric obtained in Phase I (see figure 3).

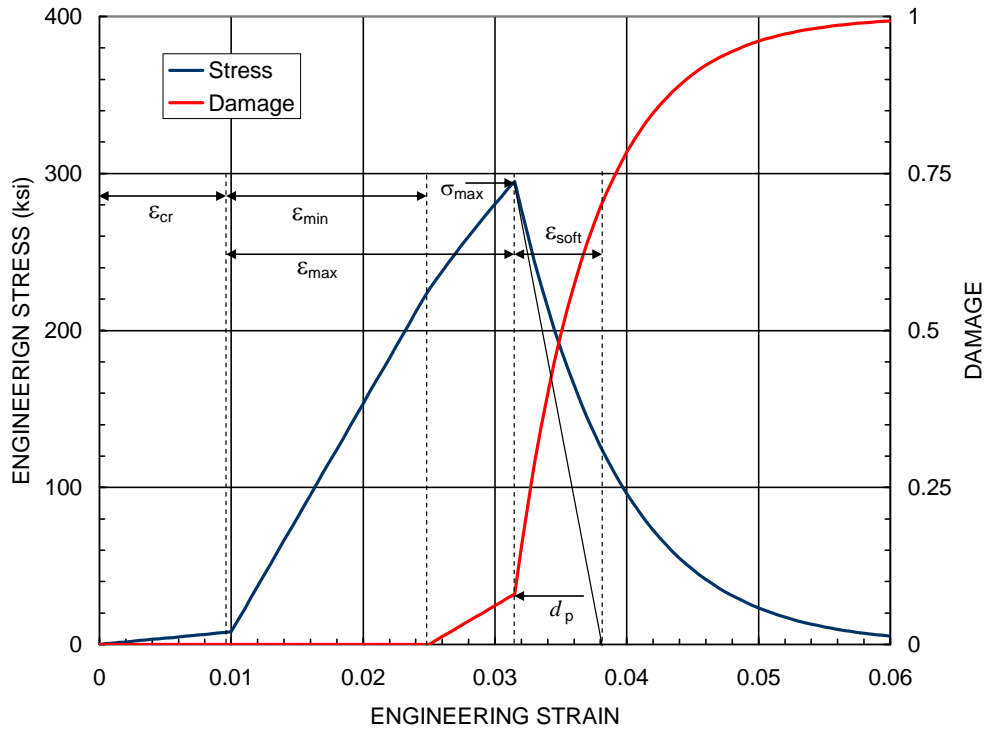


Figure 2. Damage Function for Version 1.0 for Kevlar

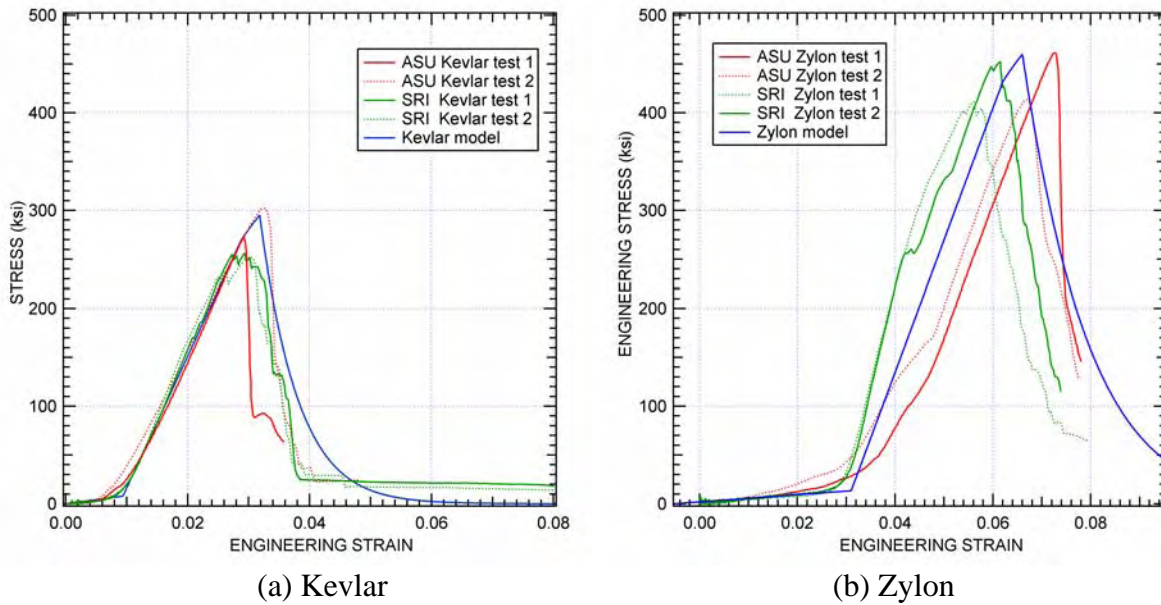


Figure 3. Test Results and Fabric Model for Phase I Uniaxial Tests

2.1.1.2 Version 1 Material Constants for Kevlar, K1A, and Zylon, Z1A.

Physical properties for 500 D Zylon as spun (AS) and 1420 D Kevlar 49 are listed in reference 3. Material properties for Version 1.0 of the fabric model for Kevlar 49 and Zylon 500 AS are listed in table 3. Note that the material constants listed in table 4 are appropriate for Versions 1.0 and 2.1 of the ballistic fabric model for the 1/4-inch mesh size used in this program. The strain associated with failure, ϵ_{soft} , and the time constant for damage are expected to be mesh size-dependent.

Table 3. Physical Properties of Zylon and Kevlar Fabrics

Trade Name		Zylon AS	Kevlar 49
Material		Polybenzobisoxazole (PBO)	P-Arimid
Volume density (from manufacturer)	(g/cm ³)	1.54	1.44
Yarn denier—as ordered	(g/9 km)	500	1420
Yarn denier—measured	(g/9 km)	500	1490
Yarn linear density—measured	(mg/cm)	0.556	1.656
Yarn cross-sectional area	(cm ² x 10 ⁻⁴)	3.61	11.50
	(in ² x 10 ⁻⁵)	5.59	17.82
Yarn count	(yarns/in.)	35x35	17x17
Fabric ply thickness (approximate)	(mm)	0.21	0.28
	(in.)	0.008	0.011
Fabric areal density—measured	(g/cm ²)	0.1575	0.02275
	(lb/ft ²)	0.0323	0.0466

Table 4. Material Constants for Kevlar (K1A) and Zylon (Z1A)

Name	Symbol	Kevlar 49	Zylon
Tensile modulus	E	10.2 Msi (70.3 GPa)	13.3 Msi (91.7 GPa)
Peak stress	σ_{max}	0.305 Msi (2.10 GPa)	0.421 Msi (2.90 GPa)
Initial damage strain	ϵ_{min}	0.0235	0.025
Strain at peak stress	ϵ_{max}	0.0262	0.036
Crimp strain x direction	ϵ_{crx}	0.01	0.037
Crimp strain y direction	ϵ_{cry}	0.01	0.006

Table 4. Material Constants for Kevlar (K1A) and Zylon (Z1A) (Continued)

Name	Symbol	Kevlar 49	Zylon
Failure strain	ϵ_{soft}	0.010	0.010
Crimp modulus	cr	0.091	0.047
Compression modulus	co	0.005	0.005
Time constant	t_c	8 μ s	2 μ s
Density	ρ	2.69e-4 lbf s ² /in ³ 2.88 g/cm ³	2.88e-4 lbf s ² /in ³ 3.08 g/cm ³
Shell thickness	t	0.0031 in./ply (0.008 cm/ply)	0.0020 in./ply (0.005 cm/ply)

Figure 3 shows the model fits to single-ply uniaxial stress tests that were performed at SRI and ASU on Zylon and Kevlar. The SRI tests were performed by pushing an impactor transversely against a 10-inch-long swath of fabric that was held at both ends. The tests at ASU were performed by gripping and pulling in-plane 12-inch-long, 2.5-inch-wide swaths of fabric. The lower peak stresses for the Kevlar tests performed at SRI may be due to failure of the yarns at the grips.

2.1.1.3 Version 1.0 Rate Dependence.

The rate dependence in Version 1.0 put a time constant on the calculation of $\bar{\epsilon}$ in each direction. For example, in any time step when the current strain ϵ_x is greater than $\bar{\epsilon}_x$, $\bar{\epsilon}_x$ increases as follows

$$\Delta\bar{\epsilon}_x = (\epsilon_x - \bar{\epsilon}_x)(1 - \exp(-dt/t_c)) \quad (3)$$

where dt is the current time step and t_c is a specified time constant. The effect of the rate dependence on the stress-strain curve is shown in figure 4. The modulus stays the same, but the peak stress and strain at peak strain increase with strain rate. Figure 5 shows calculated peak stress as a function of strain rate along with the measured data for the uniaxial stress tests described above. Note that the strain rates of interest, 100-1000/s, are well beyond the rates for the data collected in this program.

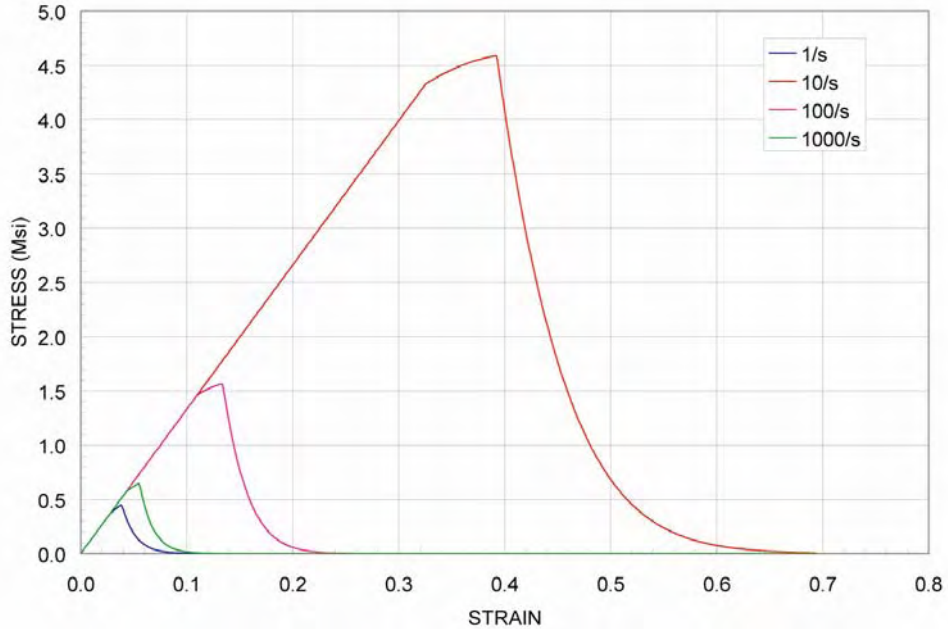


Figure 4. Stress-Strain Curves for Different Rates Version 2

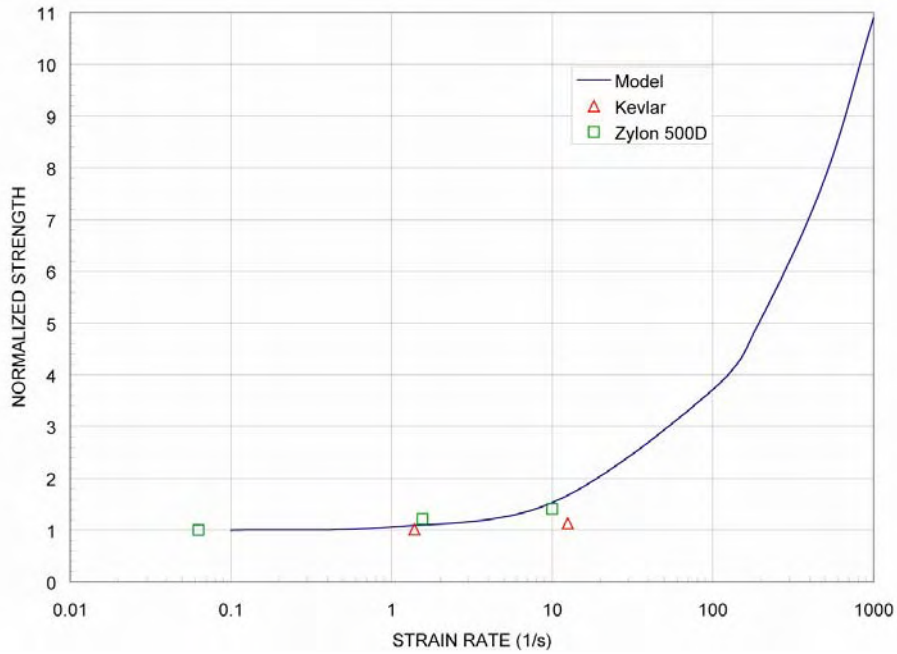


Figure 5. Rate Effect Model and Test

2.1.1.4 Failure Definition for Version 1.0.

To calculate failure in the fabric, a separate damage function was defined in each fiber direction based on the strain in that direction, and failure of the fabric was defined as complete damage occurring in either direction. For the tests performed in Phase I, that model for failure was adequate.

2.1.2 Fabric Model Version 2.

In Version 2.0, the failure definition was modified to require damage to yarns in both directions. This modification was a result of simulations of the off-design ring tests, which showed that Version 1.0 model underpredicted the strength of the fabric when the impactor was rotated 90°. Thus, in Version 2.0, to calculate damage and failure in the fabric, a separate damage function was defined in each fiber direction based on the strain in that direction, and failure of the fabric was defined as complete damage occurring in both directions. To account for the case of fabric failure by yarn pull-out, a condition was added to the model so that if the yarns failed in one direction and the stresses in the other direction are near zero, then fabric failure occurs. A change to eliminate calculation of a square root during unloading was incorporated in Version 2.1. Material model Version 2.1 was used for the parameter study described in this report.

2.1.3 Fabric Model Version 3.

Fabric Version 3 includes two models, Version 3.0 and Version 3.1. Version 3.0 is a simplified Version 3 model with a modified damage and rate dependence, but with a simplified unloading response. This version was used for development of the modified rate and damage functions, but was not used for production runs of NASA-GRC ballistic simulations. Version 3.1 is a full Version 3 with modified damage and rate dependence and full unloading response.

In all versions of the ballistic fabric model so far, rate dependence of the strength has been implemented using the concept of a time constant, i.e., that damage takes some time to develop. Thus, as the loading rate increases, the stresses in the fabric reach a higher level before the damage reduces it. This is similar to what happens to a running crack; the speed of the crack depends on the driving stress, the higher the driving stress, the faster the crack grows. But because the maximum crack speed is limited to a fraction of the Rayleigh wave velocity in the material, at high-enough strain rates, the time the crack takes to grow is large compared to the time to increase the stress.

2.1.3.1 Damage Function for Version 3.

Three problems with the fabric response for Version 2.1 were identified:

- The stress-strain curves for uniaxial tests in Phase II were much smoother than those in Phase I; i.e., the peak was not as severe as in the Phase I uniaxial tests. The damage function was modified to be smooth, as described in the section for Task 1.3.1.
- The fabric failure criterion of yarns breaking independently did not seem to be consistent with the penetrated specimens, which SRI inspected. These specimens showed that the yarns failed together; i.e., there were no specimens where the yarns in one direction failed without the yarns in the other direction breaking as well.
- The model rate dependence was not consistent with the high-rate uniaxial test results and for the NASA-GRC ballistic tests at lower velocities. Version 2 had much stronger rate dependence than the University of Washington (UW) strain rate test results, as shown in

section 3. Also, for Phase I, ballistic impact tests shot at lower velocity. This model showed a much larger reduction in strength than did the test results.

The following changes were made for Version 3: (1) the damage as a function of strain was made a smooth function, (2) fabric failure was made a function of both stresses together, and (3) the rate formulation was recast to make it less sensitive to rate in the range 1-1000/s.

2.1.3.2 Damage Function for Version 3.

To accommodate the difference in the shape of the uniaxial stress-strain curves for the Phase II tests, in the Version 3 fabric model the damage formulation was modified to be a smooth function of strain. The Version 3 damage function is given by

$$d = a \exp\left(\frac{\bar{\epsilon} - \epsilon_{\min} - \epsilon_{cr}}{\epsilon_0}\right) \quad (4)$$

where $\bar{\epsilon}$ is the strain quantity that the damage is based on and the material constants a and ϵ_0 are determined to match the input quantities ϵ_{\min} , ϵ_{\max} , σ_{\max} , and ϵ_{80} (the strain at 80% of the peak stress), as shown in figure 6.

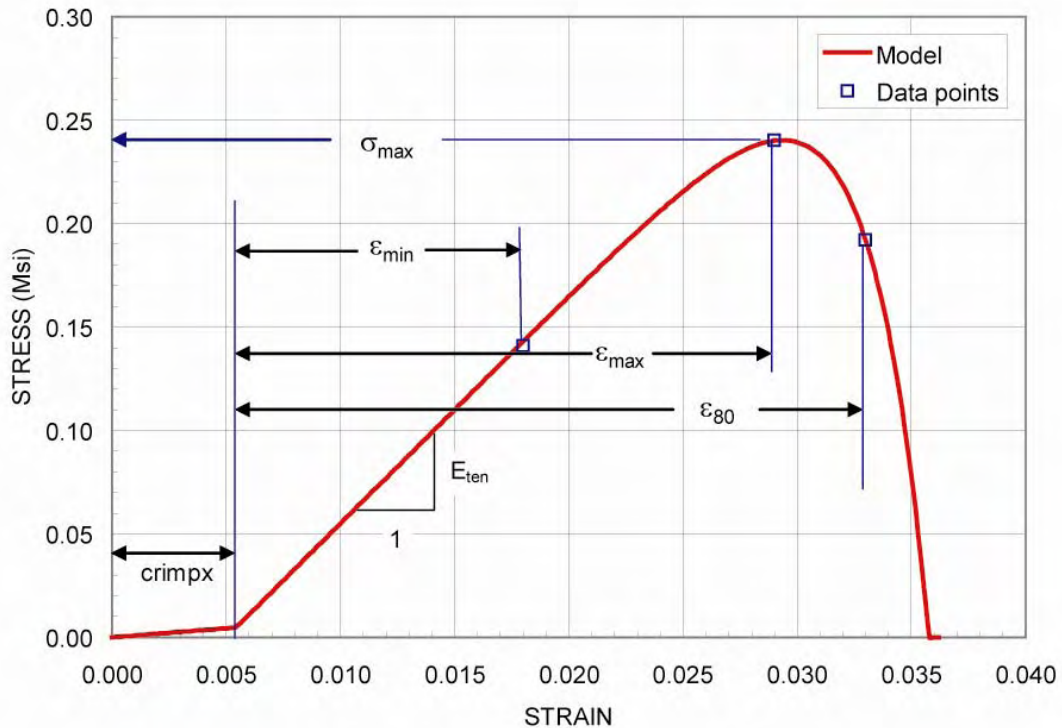


Figure 6. Version 3 Model Parameters

The resulting model for damage and stress in Kevlar is shown in figure 7.

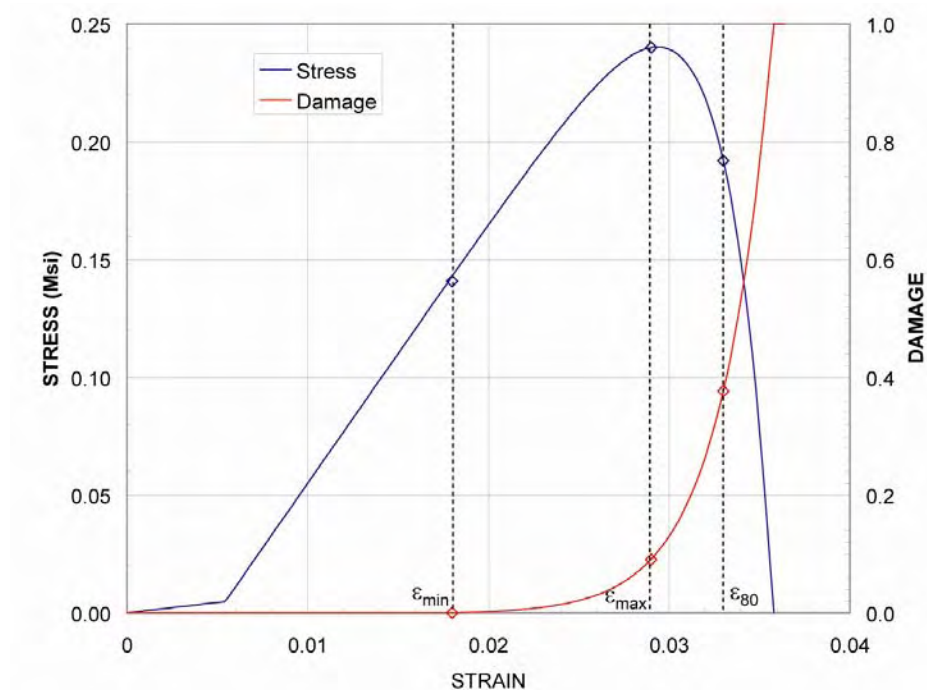


Figure 7. Version 3 Model Damage

In Version 3, the damage function was modified so that instead of tracking separate damage for the yarns in the two directions, damage is defined as a scalar function of the fiber stresses in both directions. The driving stress for the damage σ_{dr} is a norm of the current stresses in the fiber directions

$$\sigma_{dr} = (\sigma_x^n + \sigma_y^n)^{1/n}$$

where the exponent, n , is a material constant. Based on equation 3, the stress value, σ_{dam} , that corresponds to the current level of damage, d , is given by

$$\sigma_{dam} = E \left(\varepsilon_0 \ln \left(\frac{d}{a} + 1 \right) + \varepsilon_{min} \right) \quad (5)$$

2.1.3.3 Rate Dependence for Version 3.

If σ_{dr} is greater than σ_{dam} , then the damage will increase at a rate given by

$$\bar{d} = \frac{\left(\frac{\sigma_{dr}}{\sigma_{dam}} \right)^m}{t_c} \quad (6)$$

where m is a material constant, and t_c is a time constant for the damage. Values of m and t_c were chosen to match the combined rate data developed at UW. The results of strength increase as a function of strain rate are shown in figure 8. The increase in strength with rate is more gradual than for Version 1.0 (see figure 5); from rates of 1 to 100/s the strength increase is about 30%.

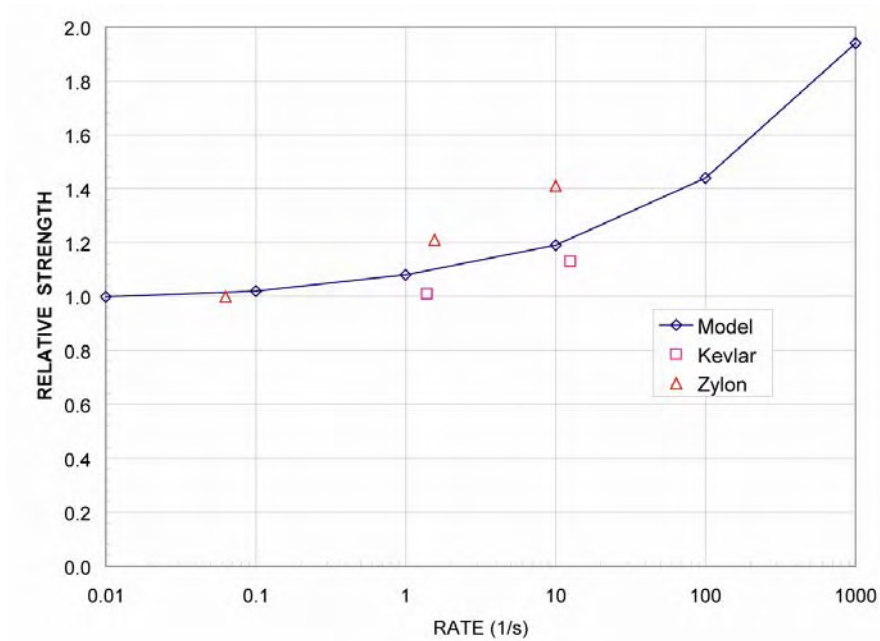


Figure 8. Rate Effect Theory Version 3

2.1.3.4 Failure in Version 3.

Element failure in Version 3 occurs as a simple function of the scalar damage parameter. When the damage value is within a small tolerance ($1.e-3$) of 1.0, the element fails and is eroded.

2.1.3.5 Material Sets K3A and Z3A.

The material constants for Kevlar as based on uniaxial tests, set K3A, are listed in table 5 and for Zylon, set Z3A are listed in table 6.

Table 5. Kevlar Material Constant Set K3A

E	ϵ_{\min}	ϵ_{\max}	σ_{\max}	ϵ_{80}	ϵ_{crx}	ϵ_{cry}	cr
11.0 Msi	0.013	0.024	0.24 Msi	0.028	0.02	0.005	0.091
t_c	m	unl	$2G$	n			
0.004	2.0	2.0	0.55	4.0			
co							
0.01							

Table 6. Zylon Material Constant Set Z3A

E	ϵ_{\min}	ϵ_{\max}	σ_{\max}	ϵ_{80}	ϵ_{crx}	ϵ_{cry}	cr
19.5 Msi	0.018	0.024	0.44 Msi	0.026	0.032	0.006	0.047
t_c	m	unl	$2G$	n			
0.0025	2.0	2.0	0.2	4.0			
co							
0.01							

2.1.3.6 Material Set K3B.

The material strength parameters for Kevlar were adjusted to better match the ring test data, as described in section 3.3.2. The values for the material constants set, K3B, are listed in table 7.

Table 7. Kevlar Material Constant Set K3B

E	ϵ_{\min}	ϵ_{\max}	σ_{\max}	ϵ_{80}	ϵ_{crx}	ϵ_{cry}	cr
11.0 Msi	0.036	0.040	0.40 Msi	0.044	0.02	0.005	0.091
t_c	m	unl	$2G$	n			
0.004	2.0	2.0	0.55	4.0			
co							
0.01							

2.1.4 Comparison of Version 3.1 to Version 1.0.

In Phase I, SRI simulated the Phase I NASA-GRC tests and compared the absorbed kinetic energy (KE) to the model and tests. Figure 9 shows the results of those simulations in terms of normalized absorbed KE along with the results of simulations using the updated Version 3.1 model for Kevlar, a single shell element layer for the fabric, and no friction between the fabric and the impactor. The Version 1.0 simulations of the 1- and 2-ply tests absorbed less energy than in the tests and less compared to the other simulations. The difference was attributed to the strong rate dependence in Version 1.0, because for the 1- and 2-ply tests, the impactor velocity (and hence, the deformation rate of the fabric) was less than half that of all the other tests (350-400 fps compared to 900 fps), which justified modifying the rate dependence for Version 3. Note that for the Version 3.1, the energy absorbed for the 1- and 2-ply tests is comparable to other simulations and is closer to the test results.

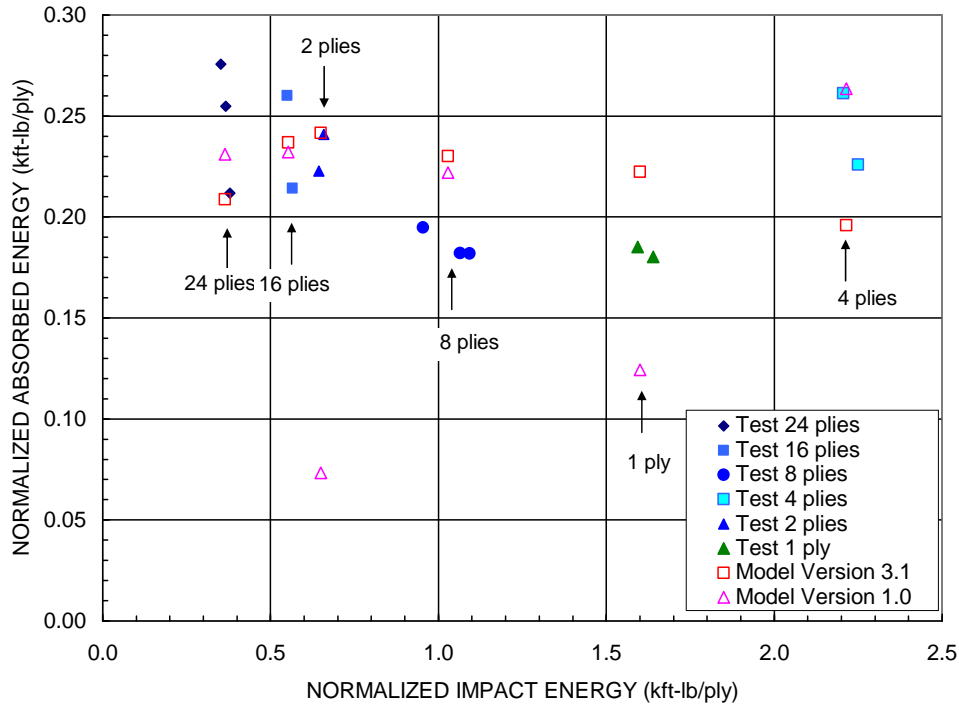


Figure 9. Comparison of Version 1.0 and Version 3.1 Simulations of Phase I NASA-GRC Tests

2.2 LS-DYNA MODEL VERSIONS.

Simulations in Phase II were run using LS-DYNA Version 970, revision 5434a, double precision, on a 32-bit Linux Workstation, Linux 2.4.20.

3. TASK 1: ROBUST FE MODEL DEVELOPMENT.

3.1 SENSITIVITY STUDY OF MODEL PERFORMANCE (TASK 1.1).

3.1.1 Test Configuration.

To increase the robustness of SRI's model for ballistic fabric, SRI performed a parameter study to quantify the effects of the material model parameters on the response of the ballistic fabric. As a test problem, SRI modeled a ballistic impact test characteristic of those performed for this program at NASA-GRC. The test setup, shown in figure 10, is a 10-inch-wide fabric swath wrapped around a 40-inch outer diameter steel ring. The ring was positioned at a 15° angle to allow the impactor to clear the steel ring and impact the center of the fabric swath from inside the steel ring. The steel ring had a 10-inch gap around the point of impact.

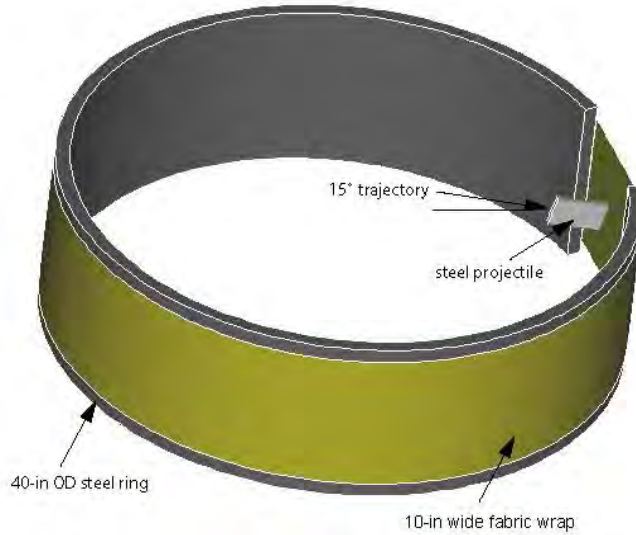


Figure 10. The NASA-GRC Test Configuration

The impactor was a 4" by 2" by 5/16" rectangular steel block with rounded edges (5/16" radius), as shown in figure 10, and with a nominal weight of 317 g. The impactor was launched from a gas gun and oriented to hit the fabric with the long side aligned with the axis of the ring, as shown in figure 11. Because the ring was positioned at a 15° angle relative to the trajectory of the impactor and the fabric was pulled tight across the gap in the ring, one corner of the impactor hit the fabric first. Results of the NASA-GRC tests are presented in Part 2 of this Phase II report.

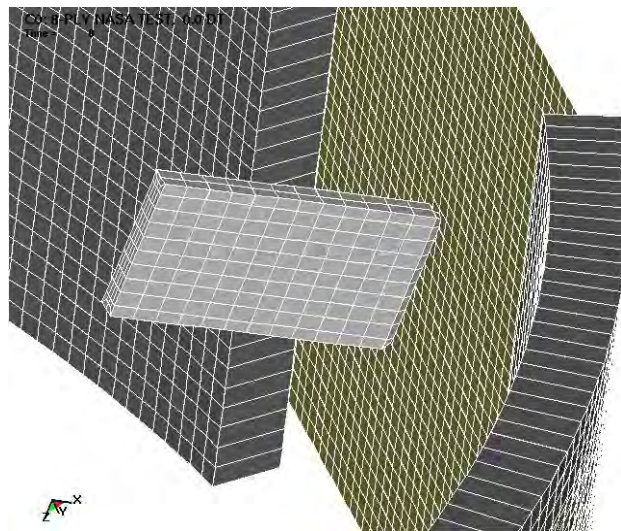


Figure 11. The FE Model of Impactor, Fabric, and Ring

In the NASA-GRC ballistic impact test series, tests were performed on Kevlar with 1, 2, 4, 8, 16, and 24 plies of fabric and for Zylon 4, 8, 16, and 24 plies. The velocity of the impactor varied from 345 to 915 ft/s. For the parameter study, SRI simulated a test on 8-ply Zylon with the velocity set at 900 ft/s.

3.1.2 The FE Model.

The FE mesh used in the simulations is shown in figure 11. One quarter inch elements were used as the standard element size. The resulting model including the ring, fabric, and impactor has about 18,000 elements. The steel ring and steel impactor were modeled as elastic. The fabric was modeled with a single layer of shell elements with the element thickness chosen to represent 8 plies of fabric.

3.1.3 Parameter Variations.

As a baseline case for the parameter study, the material set Z1A for Zylon AS was used as listed in table 4. To isolate the effects of the many parameters, the first set of parameter variations, damage, and failure of the fabric were not included. The parameters varied for the first set included: amount of crimp, shear modulus, tensile modulus, element type, unloading modulus, interface parameter SOFT, number of plies, and computational time step. Twenty-one simulations were performed; the values for the parameters are listed in table 8. Values for the various moduli are relative to the default value for tensile modulus, 13.3 Msi. Material model Version 2.1 was used for the simulations in this parameter study.

Table 8. Parameter Variations for No-Damage Simulations

Study	Case	ϵ_{crx}	$\frac{2G}{E_b}$	$\frac{E}{E_b}$ $E_b = 13.3 \text{ Msi}$	Element Type	Unl	Soft	No. Plies	Time Step
ϵ_{crx}	0	0	0.05	1.0	5	1	2	8	0.25
	1	0.01	0.05	1.0	5	1	2	8	0.25
	2	0.05	0.05	1.0	5	1	2	8	0.25
	3	0.10	0.05	1.0	5	1	2	8	0.25
$\frac{2G}{E_b}$	4	0	0.01	1.0	5	1	2	8	0.25
	5	0	0.02	1.0	5	1	2	8	0.25
	6	0	0.05	1.0	5	1	2	8	0.25
	7	0	0.05	1.0	5		2	8	0.25
$\frac{E}{E_b}$	8	0	0.05	2.0	5	1	2	8	0.25
	9	0	0.05	0.5	5	1	2	8	0.25
Element Type	10	0	0.05	1.0	2	1	2	8	0.25
	11	0	0.05	1.0	16	1	2	8	0.25
	12	0	0.05	1.0	9	1	2	8	0.25
Unl	13	0	0.05	1.0	5	2	2	8	0.25
	14	0	0.05	1.0	5	1.5	2	8	0.25
Soft	15	0	0.05	1.0	5	1	1	8	0.25
	16	0	0.05	1.0	5	1	0	8	0.25

Table 8. Parameter Variations for No-Damage Simulations (Continued)

Study	Case	ϵ_{crx}	$\frac{2G}{E_b}$	$\frac{E}{E_b}$ $E_b = 13.3 \text{ Msi}$	Element Type	Unl	Soft	No. Plies	Time Step
No. Plies	17	0	0.05	1.0	5	1	2	24	0.25
	18	0	0.05	1.0	5	1	2	16	0.25
Time Step	19	0	0.05	1.0	5	1	2	8	0.50
	20	0	0.05	1.0	5	1	2	8	0.0

To make the comparison between the different cases, the stress developed in the first element impacted by the impactor was examined. Usually, the first element impacted was the element that failed first. Once one element fails, the impactor usually penetrates the fabric. Figure 12 shows the element stress and the impactor velocity for the baseline case. As listed in table 8, the baseline case is linear orthotropic, with no crimp, tensile modulus as measured in the static tests, a shear modulus 5% of the tensile modulus, unloading modulus equal to the tensile modulus, element type 5, and time step of 0.2 times the default time step (based on the time it takes a pressure wave to cross the smallest element dimension).

3.1.4 Baseline.

As shown in figure 12, the character of the element stress is an initial pulse of stress to 0.45 Msi upon impact, then a stress rise to a peak of about 0.7 Msi at about 0.1 ms after impact, followed by a drop in stress to fairly constant oscillations between 0.4 and 0.5 Msi at 50 kHz, followed by a second stress drop at about 0.4 ms after impact. Under static testing, the peak strength of Zylon is about 0.42 Msi, so the element stress for this set of parameters is greater than the static strength for much of the first 0.4 ms.

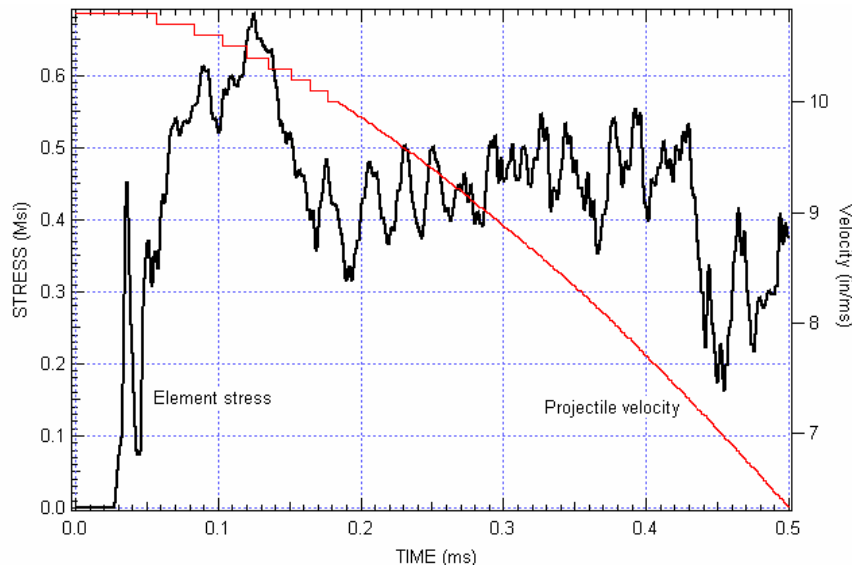


Figure 12. Baseline Case

One interesting result observed was that the character of the element stress history changed at about 0.1 ms from a smoothly varying curve to a rough curve (this effect is clearer in figure 13). The cause of this effect is unknown.

The calculated impactor velocity history is also shown in figure 12. From the initial velocity of 10.8 in./ms, the velocity steadily decreased to about 6.3 in./ms at 0.5 ms. For the 8-ply cases, the average residual velocity for the tests was about 9.5 in./ms, which suggests that the impactor penetrated the fabric at about 0.2 ms after impact, which is after the stress has dropped from the peak.

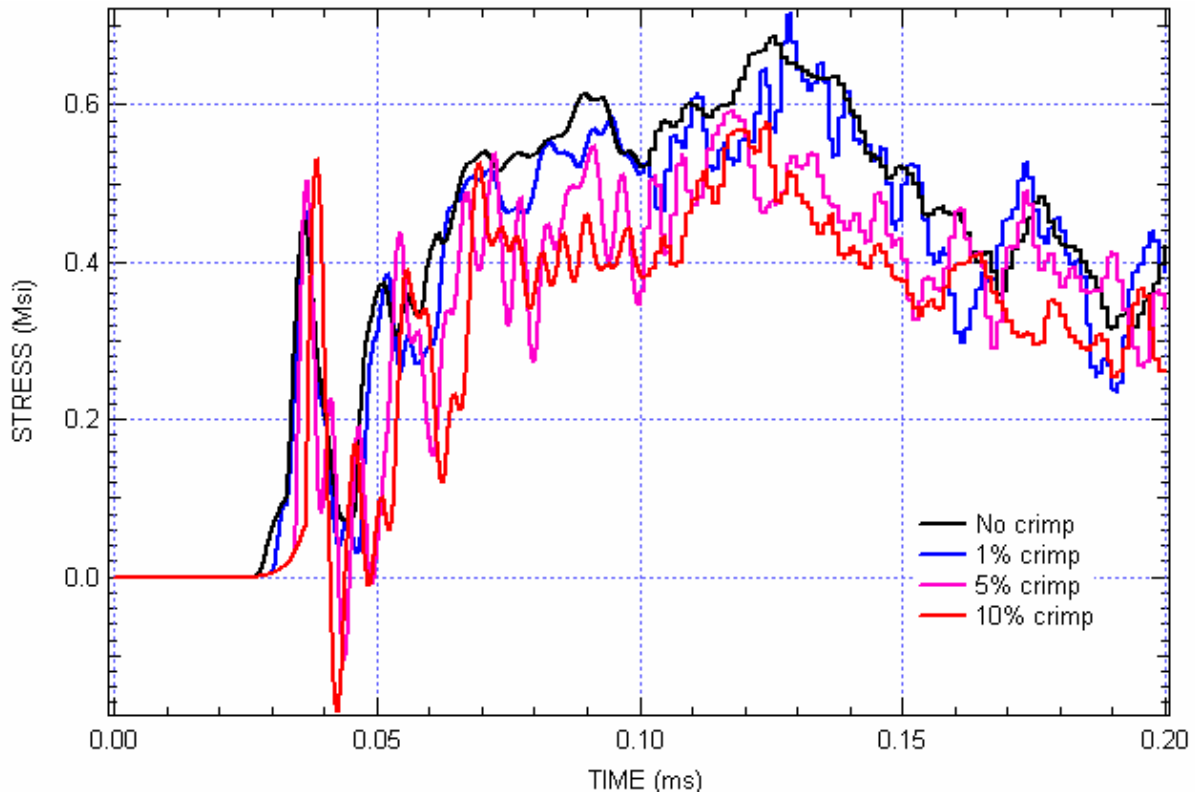


Figure 13. Effect of Crimp

3.1.5 Measured Parameters (Task 1.1.1).

3.1.5.1 Crimp.

The effect of crimp on the response is shown in figure 13. Along with the baseline case with no crimp (C0), three cases of crimp (C1, C2, and C3) were simulated with 1%, 5%, and 10% crimp, respectively. In general, the effect of increasing the crimp was to increase the dynamic overshoot of the initial impact, as well as to increase the magnitude of early time oscillations, and to decrease the stress level at later times. One significant effect was that for crimp values of 5% and 10%, the rebound from the initial impact goes into compression. (To limit the number of parameters for this first set of simulations, it was assumed the fabric could take compressive loads).

3.1.5.2 Tensile Modulus.

There is a clear and significant effect on stress with variations in the tensile modulus. Increasing the tensile modulus increases the stresses, and decreasing the tensile modulus reduces the stresses. Results for cases C8 and C9 are shown in figure 14. Doubling the tensile modulus increased the stresses by about 25%, and halving the tensile modulus decreased the stresses by about 25%.

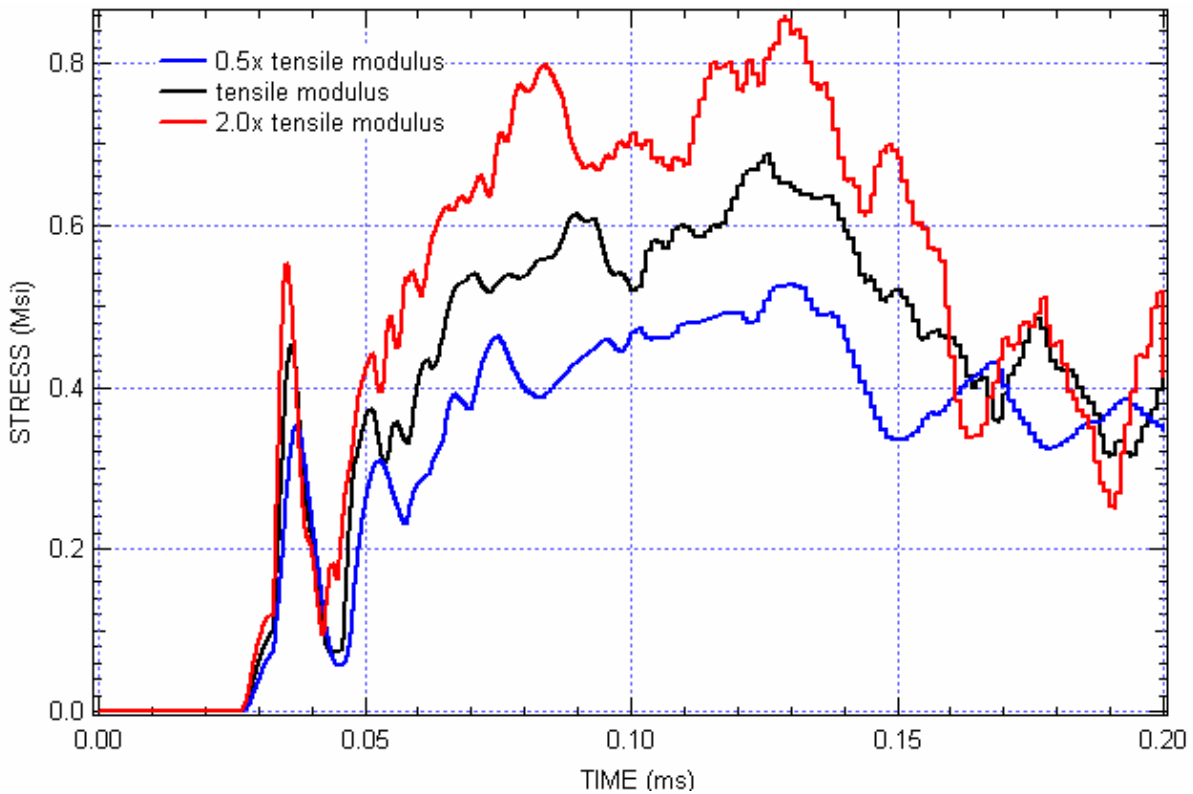


Figure 14. Effect of Variations in Tensile Modulus

3.1.5.3 Unloading Modulus.

The effect of the unloading modulus was investigated in cases C12 and C13. The baseline case had the unloading modulus equal to the tensile modulus. In the static tests, the measured unloading modulus in cyclic tests was about twice the tensile modulus. The results of the simulations, shown in figure 15, show very little effect of unloading modulus on the stress response.

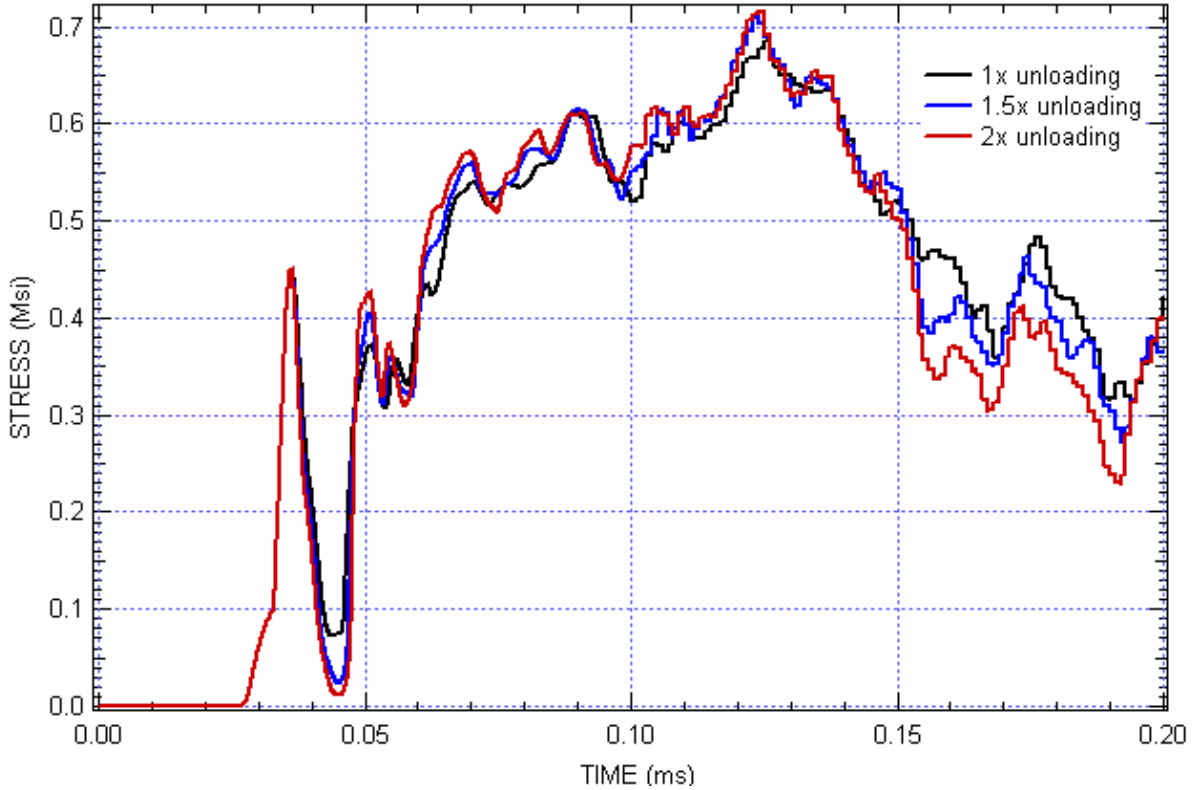


Figure 15. Effect of Variations in Unloading Modulus

3.1.6 Estimated Parameters (Task 1.1.2).

3.1.6.1 Shear Modulus.

Although there were no measured values available for shear modulus, it was assumed that for bare fabric the shear modulus (which is the resistance to the yarns in the fabric changing relative angle to each other) is small compared to the tensile modulus. However, if the shear modulus is taken as too small a number, the FE analysis will have numerical stability problems.

For the baseline case (C0), it was assumed that the shear modulus was 5% of the tensile modulus. For cases C4-C7, the shear modulus was set to 1%, 2%, 10%, and 20% of the tensile modulus. The effect of shear modulus on the response, as shown in figure 16, is significant. The overall trend is that increasing the shear modulus increases the stresses in the fabric. Increasing the shear modulus from 5% to 10% increased the stresses in the fabric by about 25%. Increasing the shear modulus to 20% of the tensile modulus increased the element stresses by about 50% over the baseline values. Decreasing the shear modulus reduced the stresses. Surprisingly, the responses for 1% and 2% were nearly the same, with stresses about half the baseline case.

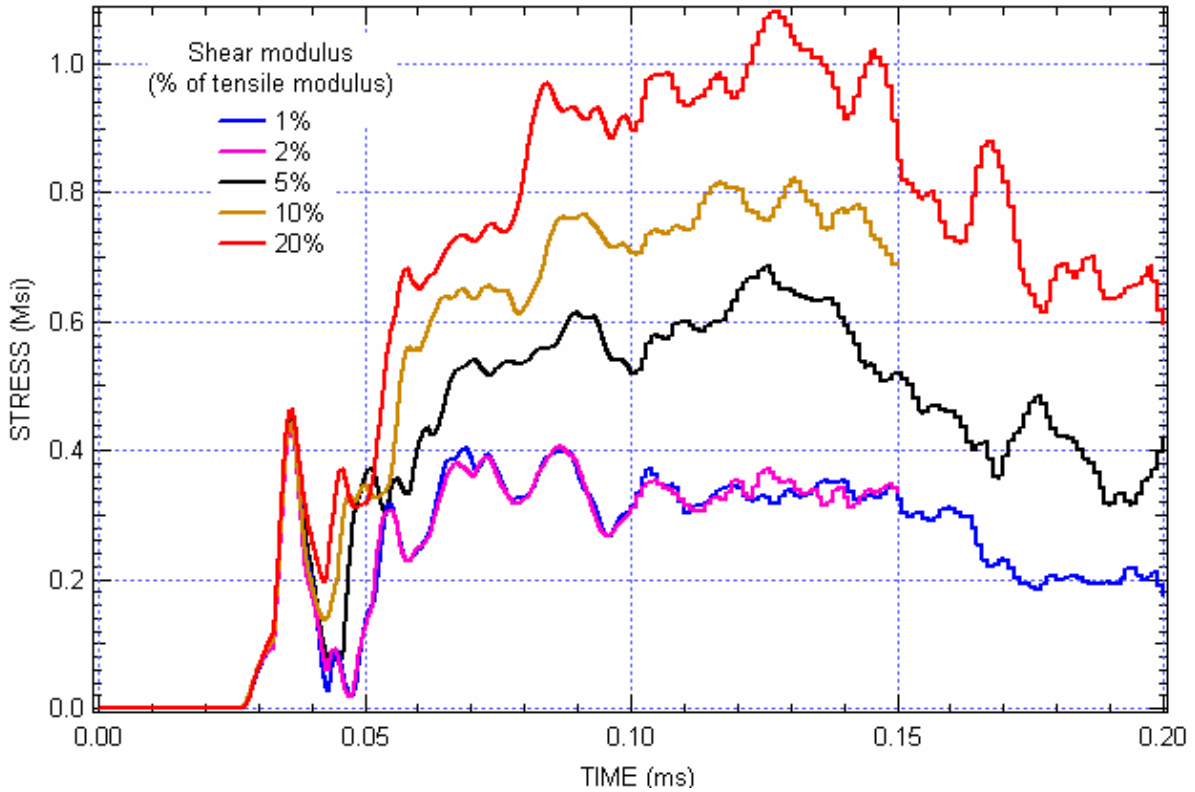


Figure 16. Effect of Variations in Shear Modulus

3.1.7 Strain Rate Dependence of Failure (Task 1.1.3).

The strain and strain rate of the first element contacted for the baseline case are shown in figure 17. Initially, the strain rate jumped to over 4000/s as the 0.037 crimp strain straightened out. During the stressing of the fabric, (i.e., for strains from 0.037 to 0.055), the strain rate averages about 150/s and ranges between about 4 and 400/s.

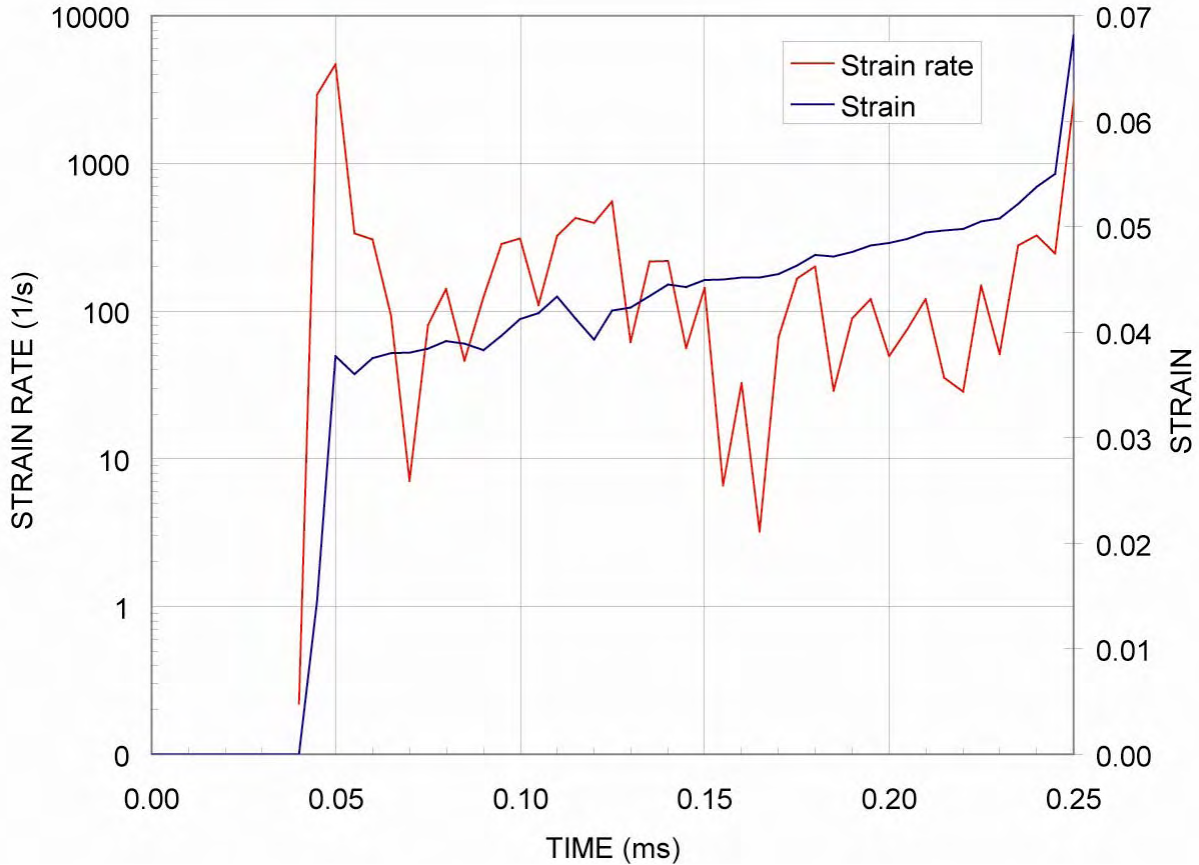


Figure 17. Element Strain Rate History

3.1.8 Numerical Considerations (Task 1.1.4).

3.1.8.1 Mesh Resolution.

An investigation of the effect of mesh resolution on the response of the fabric for the NASA-GRC ballistic testing was performed at George Washington University (GWU). NASA-GRC test LG6111 (an 8-ply Zylon test with an impact velocity of 906 ft/s (10.87 in/ms) and a residual velocity of 798 ft/s (9.58 in./ms)) was simulated. Simulations were run with the baseline (1/4" mesh), two coarser meshes that were 2 times and 4 times coarser (1/2" and 1" square), and two finer meshes, 0.5 times and 0.25 times coarser (1/8" and 1/16").

The velocity histories are shown in figure 18. There were significant differences between the results. The general trend was that the finer the mesh, the less energy absorbed. This effect can be explained by two considerations. First, finer meshes will pick up the stress gradients with higher resolution. Thus, the element stresses around the impactor are higher for a fine mesh, so those elements fail sooner. Second, because the model exhibits softening, the strain localizes in a narrow band of elements, often in a single row of element. Smaller elements absorb less energy during failure.

UMAT – V3

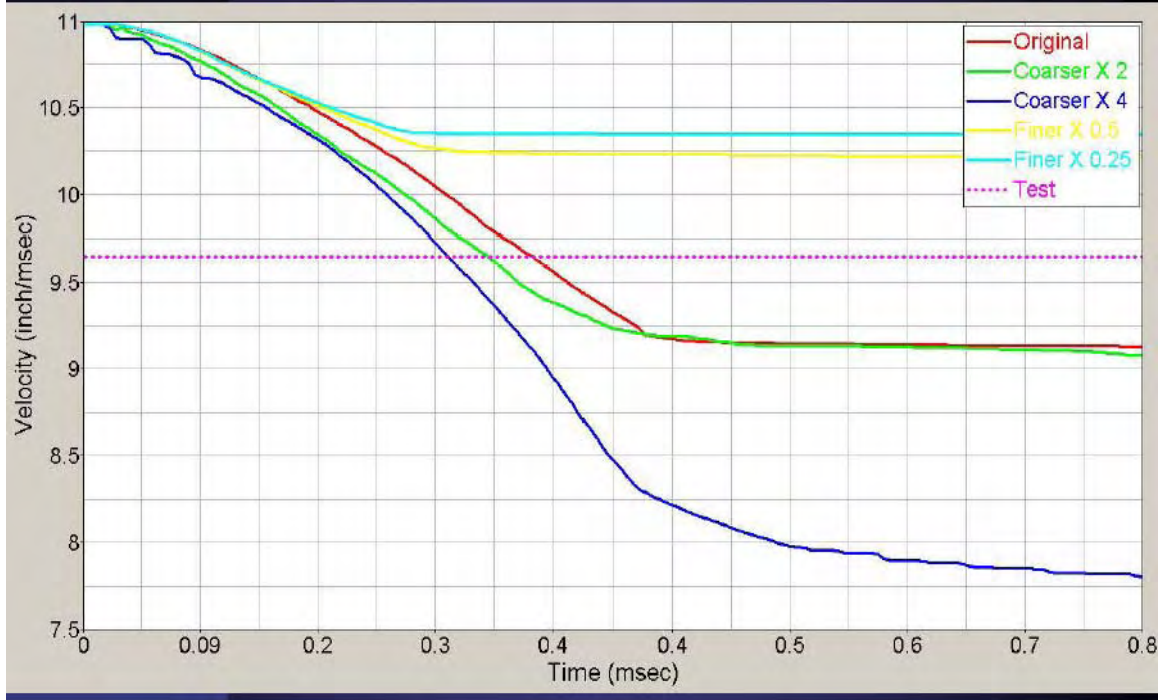


Figure 18. Mesh Resolution Simulations

3.1.8.2 Element Types.

Figure 19 shows the effect of different shell element types. In all cases, single point integration was used through the element thickness to eliminate any bending stiffness. For the baseline case, element type 5 was used (Belytschko-Tsay membrane element). Cases C10-C12 used element type 2 (default Belytschko-Tsay shell element), element type 16 (fully integrated shell element), and element type 9 (fully integrated Belytschko-Tsay membrane). Choice of element has a strong effect on the initial stress pulse. Compared to the baseline case, the initial peak stress for element type 9 was approximately 90%, type 2 was 50%, and type 16 was 35% the baseline value. Throughout the rest of the history, the stresses varied by $\pm 15\%$ and the relative magnitudes for the different element type changed within those bounds. The character of the histories was similar, although element type 2 had greater oscillations than the other element types.

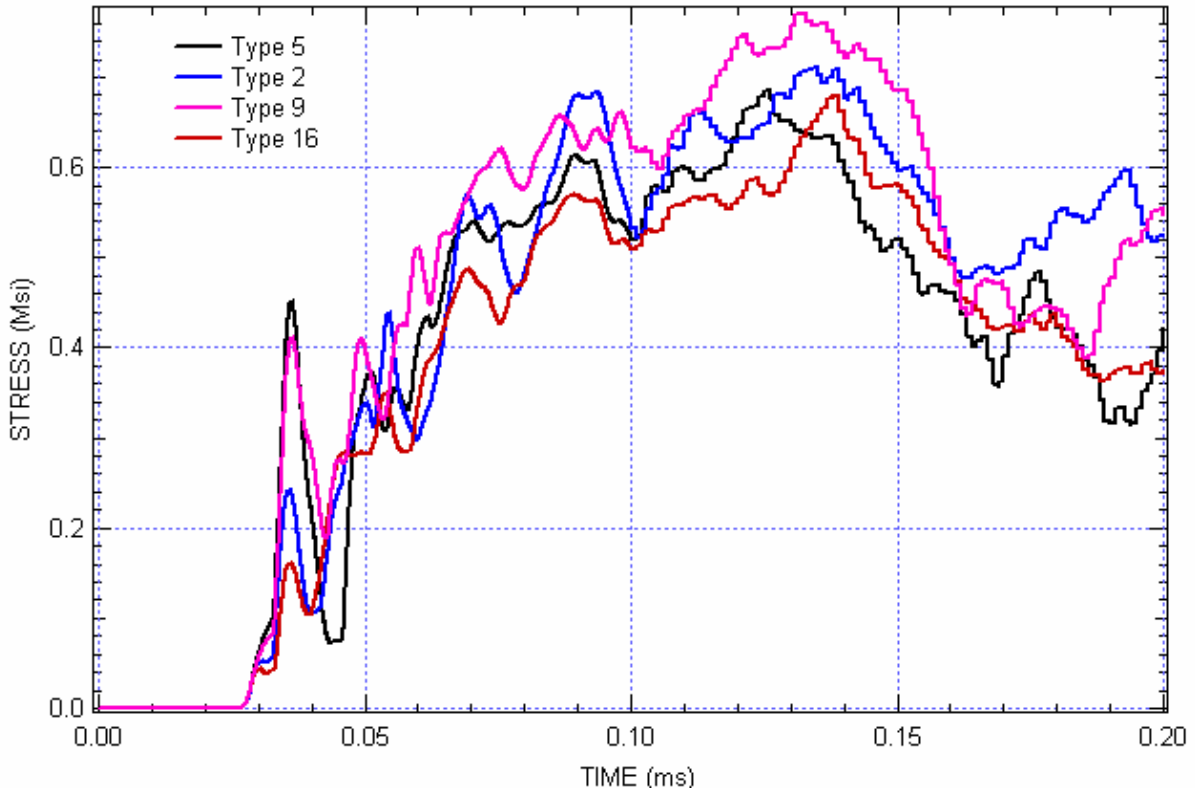


Figure 19. Effect of Variations in Element Type

3.1.8.3 Time Step.

The effect of variations in the time step is shown in figure 20. In Phase I, it was determined that reducing the time step improved the results compared to the experiments. The baseline time step was set to 0.25 times the default time step, based on the time it takes a pressure wave to cross the smallest element. For case C19, the time step was set to 0.5 times the default and for case C20, the default time step was used. The variations in time step resulted in stresses that varied by approximately 10%. In general, the larger the time step, the greater the oscillations were in the response.

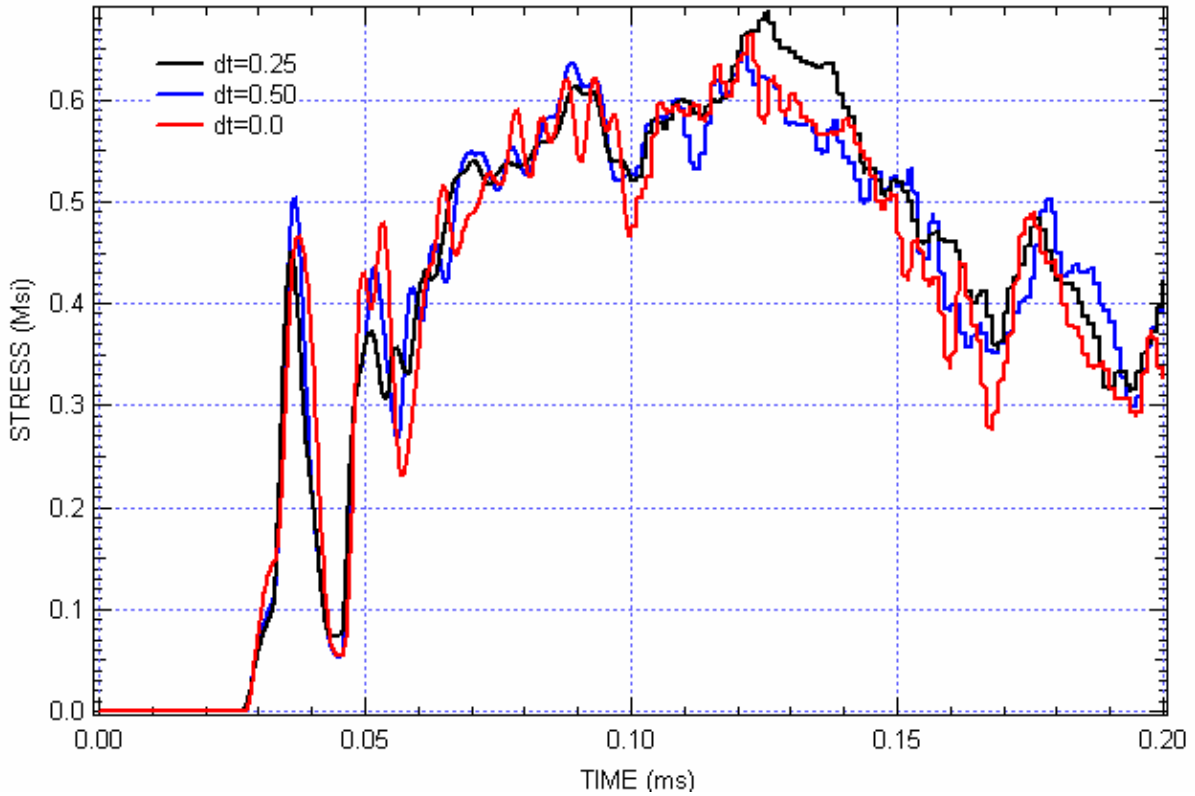


Figure 20. Effect of Variations in Time Step

3.1.8.4 SOFT Values.

Cases C14 and C15 investigated the effect of the LS-DYNA interface parameter SOFT. This parameter specifies the method for determining whether surfaces have come into contact. The baseline value is SOFT=2, which was determined in the previous program to give the best results. The results for SOFT=1 and SOFT=0 (LSDYNA default value) are shown in figure 21. There is not much difference in the response for SOFT=1 and SOFT=2; however for SOFT=0, the impactor passes through the fabric (without breaking the fabric) at a time of about 0.1 ms.

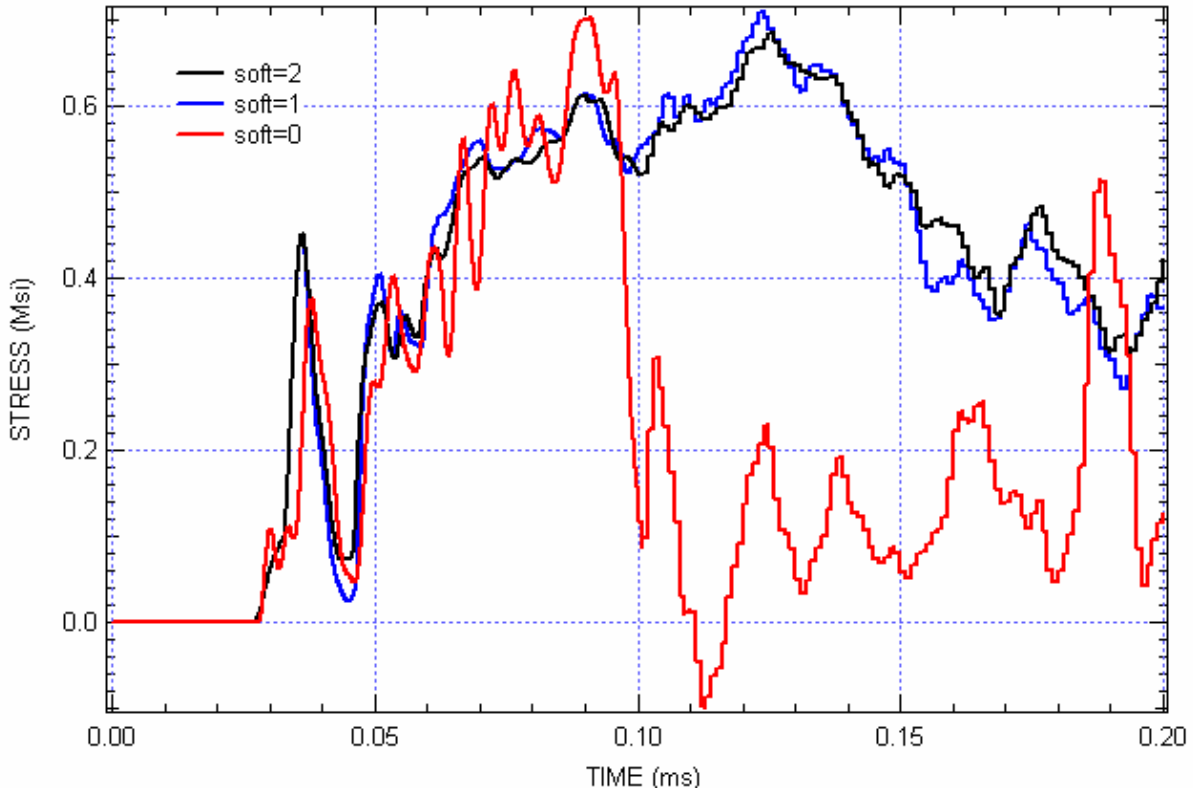


Figure 21. Effect of Variations in Slideline Parameter Soft

3.1.8.5 Number of Plies.

Figure 22 shows the results of variations in the number of plies. There is very little difference in the calculated element stress for 8, 16, and 24 plies for the first 0.2 ms of the response. In the tests on Zylon, the impactor penetrated the fabric for 8 and 16 plies but not for 24 plies. From these calculated stress histories, combined with the observation from figure 12 that the impactor penetrated 8 plies within 0.2 ms, it is difficult to explain the test results in terms of element stresses. As described in section 4.1, multilayer fabric targets appear to fail progressively, with the impacted layers failing first and the outer layers failing later. So, in multilayer targets that were not penetrated, the inner layers were fully penetrated, the middle layers were penetrated by the corners of the projectile, and the outer layers were not penetrated at all. Thus, treating the multiple layers with more than a single element through the thickness is necessary to correctly model the failure response for partially penetrated targets.

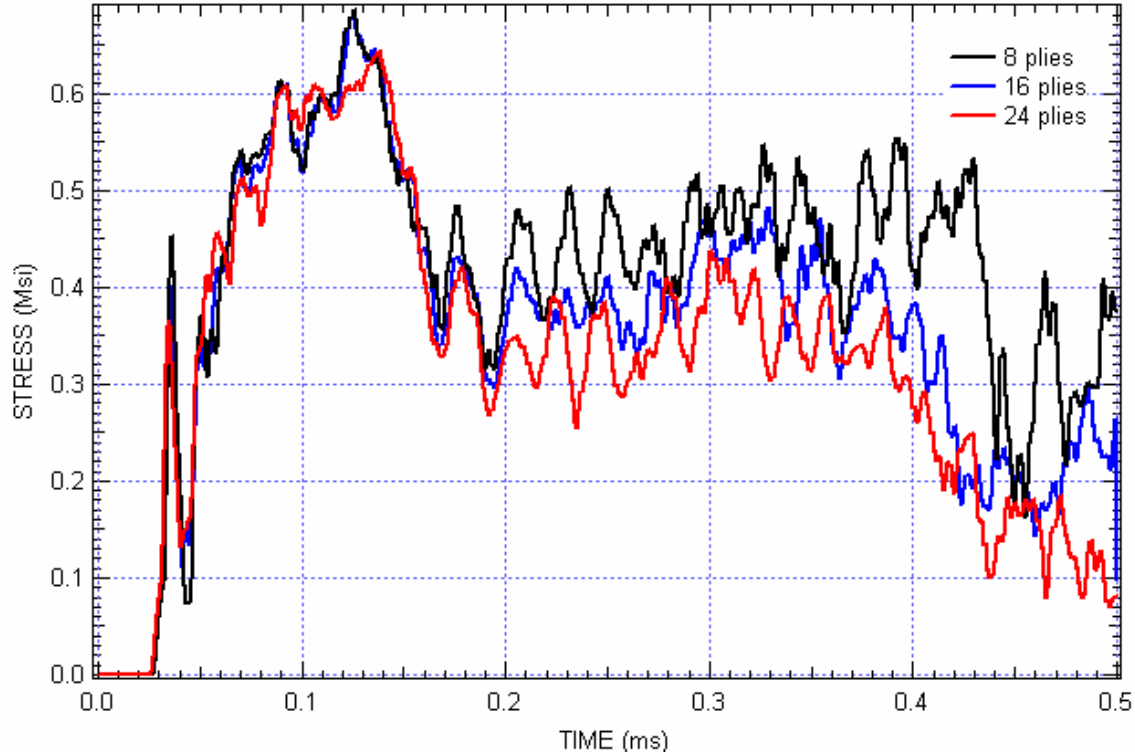


Figure 22. Effect of Variations in Number of Plies

3.1.9 Failure Parameters.

Parametric calculations investigating the effects of various failure parameters on the response of the ballistic fabric were performed. As shown in table 9, seven simulations investigating the effects of strain to failure, time constant for failure, and fabric strength were performed. Unlike the comparisons of stress histories for parameter studies without failure, for the cases with failure, it was possible to compare energy absorbed as the metric for how much effect these parameters had on the fabric response.

Table 9. Parameter Study for Failure Parameters

Study	Case	Peak Stress (Msi)	Initial Damage Strain	Strain at Peak Stress	Failure Strain	Time Constant (ms)	Residual Velocity (in./ms)	Energy Absorbed (KJ/cm)
Baseline	21	0.421	0.025	0.036	0.010	0.002	10.28	2.20
Failure strain	22	0.421	0.025	0.036	0.020	0.002	10.15	2.73
	23	0.421	0.025	0.036	0.005	0.002	10.68	0.52
Time constant	24	0.421	0.025	0.036	0.010	0.004	10.10	2.93
	25	0.421	0.025	0.036	0.010	0.001	10.29	2.16
Strong/weak	26	0.488	0.030	0.041	0.010	0.002	9.65	4.71
	27	0.355	0.020	0.031	0.010	0.002	10.43	1.59

The results show that the response of the fabric is strongly dependent on all the failure parameters, the strain to failure, time constant, and fabric strength, but more so in one direction than the other.

3.1.9.1 Strain to Failure.

The strain to failure parameter, ϵ_{soft} , is a measure of the strain to failure after the peak stress is reached, as shown in figure 2. This is a measured parameter that typically depends on the type of test performed and the compliance of the testing machine. So, although it is a measurable parameter, it is difficult to argue that it is a material parameter if it is taken from static uniaxial tension tests. As shown in figure 23, from the baseline value for failure strain of 0.010 (C21), increasing the failure strain to 0.020 (C22) increased the energy absorbed by 24% and decreasing the failure strain from 0.010 to 0.005 (C23) reduced the energy absorbed by nearly 80%.

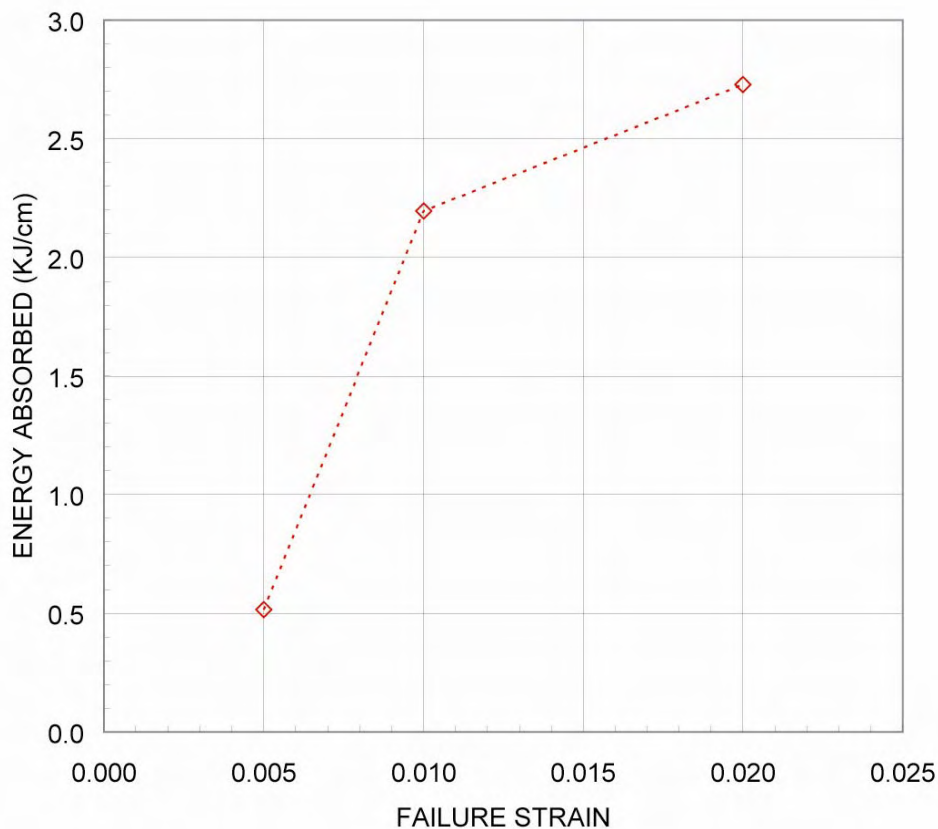


Figure 23. Effect of Failure Strain on Energy Absorbed

3.1.9.2 Time Constant.

The time to failure is a parameter that was introduced to describe rate dependence of damage and failure, namely that Kevlar and Zylon increase in strength when tested at a high rate. As shown in figure 24, from a baseline value of 0.002 ms, doubling the time constant to 0.004 ms (C24) increased the energy absorbed by 33%, but halving the time constant to 0.001 ms in (C25) decreased the energy absorbed by only 2%.

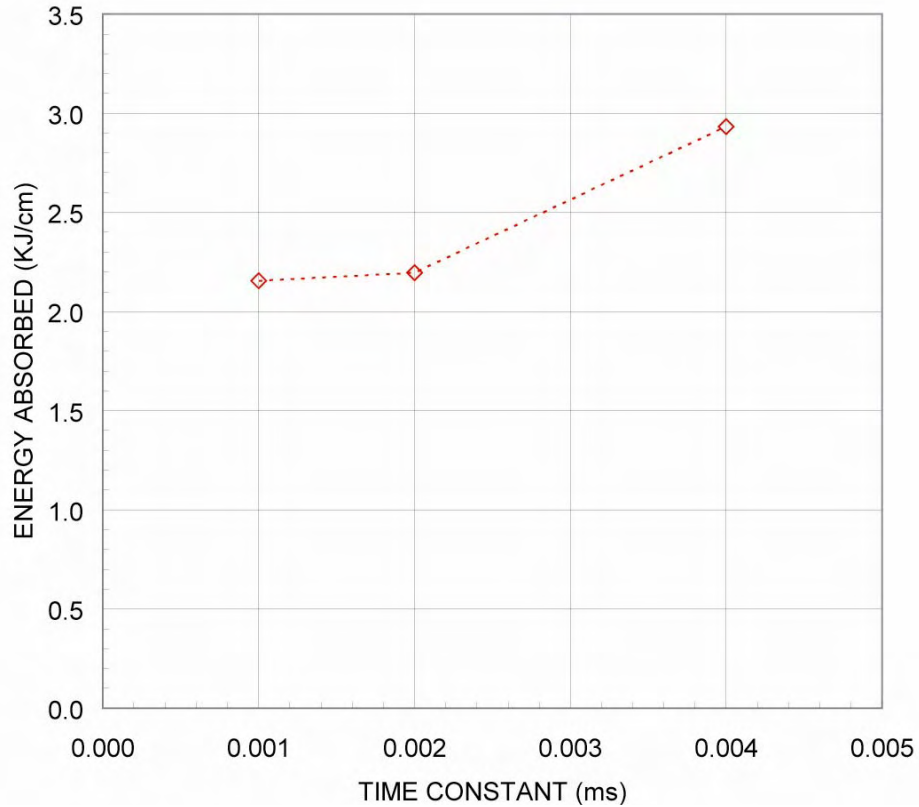


Figure 24. Effect of Time Constant on Energy Absorbed

3.1.9.3 Fabric Strength.

In C26 and C27, the effect on energy absorbed by increasing the strength of the fabric was investigated. To adjust the strength of the fabric, the values of the strain at initial damage and the strain at peak stress were shifted by 0.005, as shown in figure 25. For C26, the strain at initial damage was increased from 0.025 to 0.030 and the strain at peak stress from 0.036 to 0.041. For C26, the peak stress increased 16%, from 0.421 Msi to 0.488 Msi, and for C27 the peak stress decreased 16% to 0.355 Msi. In terms of strain energy (the area under the stress-strain curve), C27, with 0.0169 Msi, has 24% more strain energy than the baseline value of 0.0137 Msi, and with 0.0109 Msi, has 21% less strain energy. In terms of energy absorbed, as shown in figure 26, C26 absorbed 2.14 times as much energy as the baseline case, and C27 absorbed 28% less energy than the baseline case.

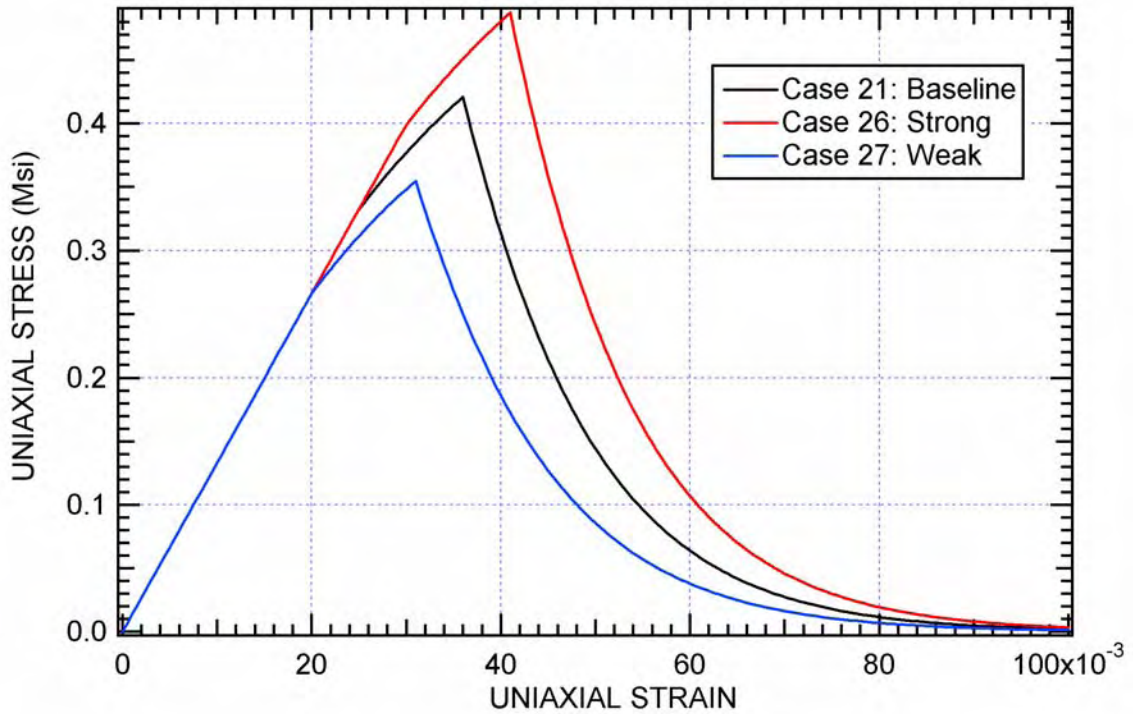


Figure 25. Stress-Strain Curves for Cases 26 and 27

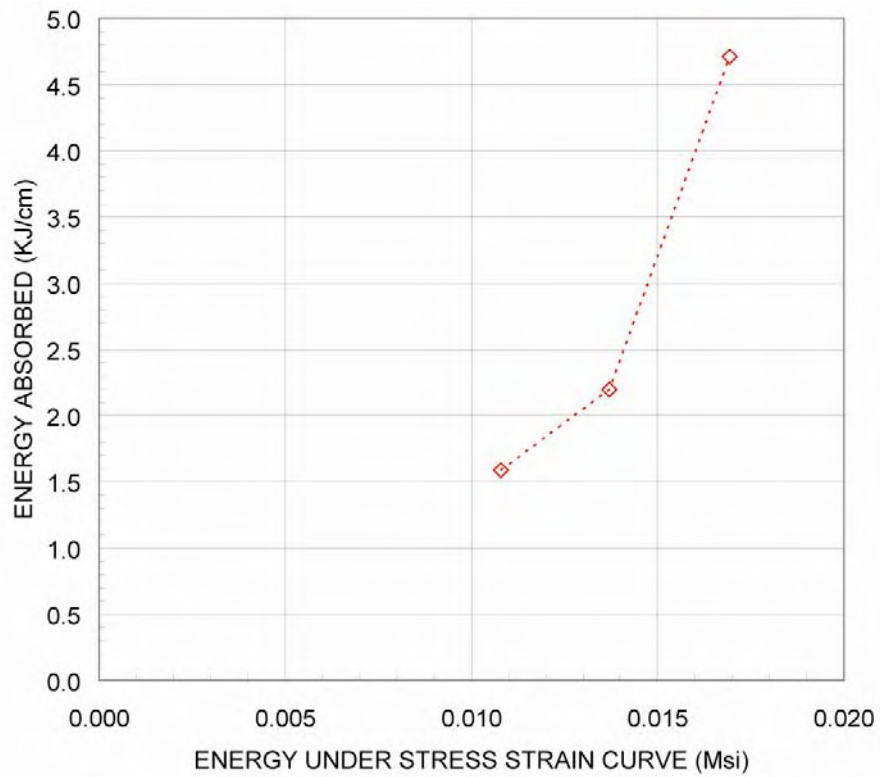


Figure 26. Effect of Material Strength on Energy Absorbed

3.1.10 Friction.

In the baseline case, as well as in almost all other simulations performed, no friction in the contact formulation was assumed. That is, it was assumed there was no friction between the impactor and the fabric and, for cases where the fabric was modeled using multiple shell layers, no friction between the fabric layers. To quantify the effect of friction, a series of simulations was performed for the Phase I tests on Zylon with 4, 8, and 16 plies, first with no friction, then assuming a friction coefficient of 0.2. In these cases, multiple shell layers were used to model the fabric; a single shell layer was used for every 4 plies of Zylon, so that 8 plies used 2 shell layers, and 16 plies used 4 shell layers. Figure 27 shows the calculated absorbed energy normalized by the number of fabric plies. In the three simulated tests, the effect of including a 0.2 coefficient of friction increased the absorbed energy by 10% to 15%.

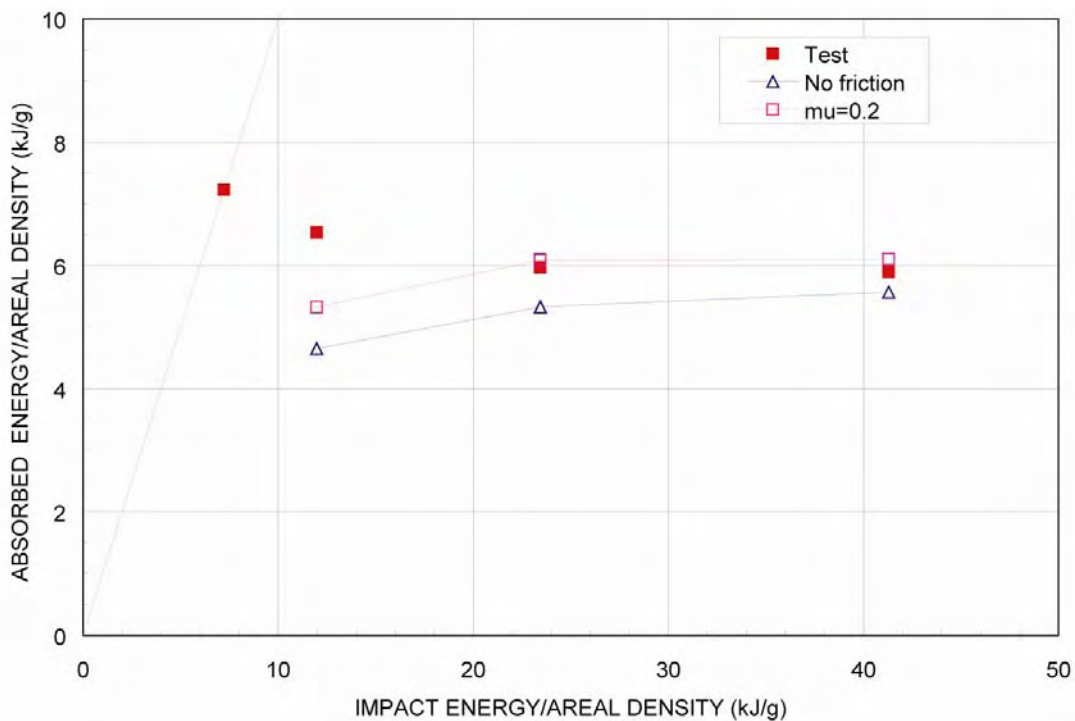


Figure 27. Effect of Friction

3.1.11 Summary.

Two sets of simulations were performed to quantify the effects of the material parameters on the ballistic response of fabric. In the first set, cases 1-20, the following parameters were varied without allowing the fabric to fail: amount of crimp, shear modulus, tensile modulus, element type, unloading modulus, interface parameter SOFT, number of plies computational time step, and mesh resolution. The results show that:

- For measured parameters, the tensile modulus has a significant effect on stresses; increasing the crimp changes the character of the response (more oscillations but lower overall stresses), but the unloading modulus has only a small effect.

- For estimated parameters, the shear modulus has a significant effect on the stresses.
- For numerical parameters, the time step has a small effect (this may change for cases with failure), the slideline parameter SOFT must equal 1 or 2 to adequately model the contact, and the element type makes a 10% to 15% difference in the stresses. Mesh resolution has a significant effect on energy absorbed, with the trend being the finer the mesh, the less the energy absorbed. For test LG611, decreasing the mesh resolution by 2 decreased the energy absorbed from 30% to 13%.
- The number of plies has a very little effect on the stresses up to 0.2 ms after impact.

In the second set of simulations, cases 21-27, the following failure parameters were varied: failure strain, time constant, and fabric strength. The results of simulations including failure show that:

- Variations in the failure strain can have a significant effect on energy absorbed. Doubling the failure strain from 0.01 to 0.02 increased the energy absorbed by 24%, decreasing it by half decreased the energy absorbed by 80%.
- Doubling the time constant increased the energy absorbed by 33%, but decreasing it by half decreased the energy absorbed by only 2%.
- Increasing the fabric strength had a strongly nonlinear effect on energy absorbed. Increasing the peak stress by 16% increased the energy absorbed by greater than a factor of 2 (2.14), but decreasing the strength 16% decreased the energy absorbed by only 28%.

Overall, it is difficult to explain all the nonlinear dependence of the response on the material parameters. One possible explanation has to do with time to failure; that is, once a failure initiates, it quickly propagates and no more energy is absorbed. Considering the failure can initiate either by sudden peaks of stress or by long-time overall straining, changes in material properties that allow the fabric to withstand initial peaks of stress can make significant differences in energy absorbed.

The effect of including friction in the contact algorithm is to increase the amount of absorbed energy. A coefficient of friction of 0.2 increased the energy absorbed by 10% to 15%.

3.2 TENSION TESTING (TASK 1.3).

3.2.1 Simple Tension Testing (Task 1.3.1).

Results of uniaxial stress-strain tests on 1420 D Kevlar 49 and 500 D Zylon conducted at ASU for Phase II are shown in figure 28. Compared to the results of Phase I (see figure 3), these curves are smoother in the region around the peak stress. The model simulations using Version 3.1-K3A for the Kevlar and Version 3.1-Z3A for the Zylon are also shown in figure 28.

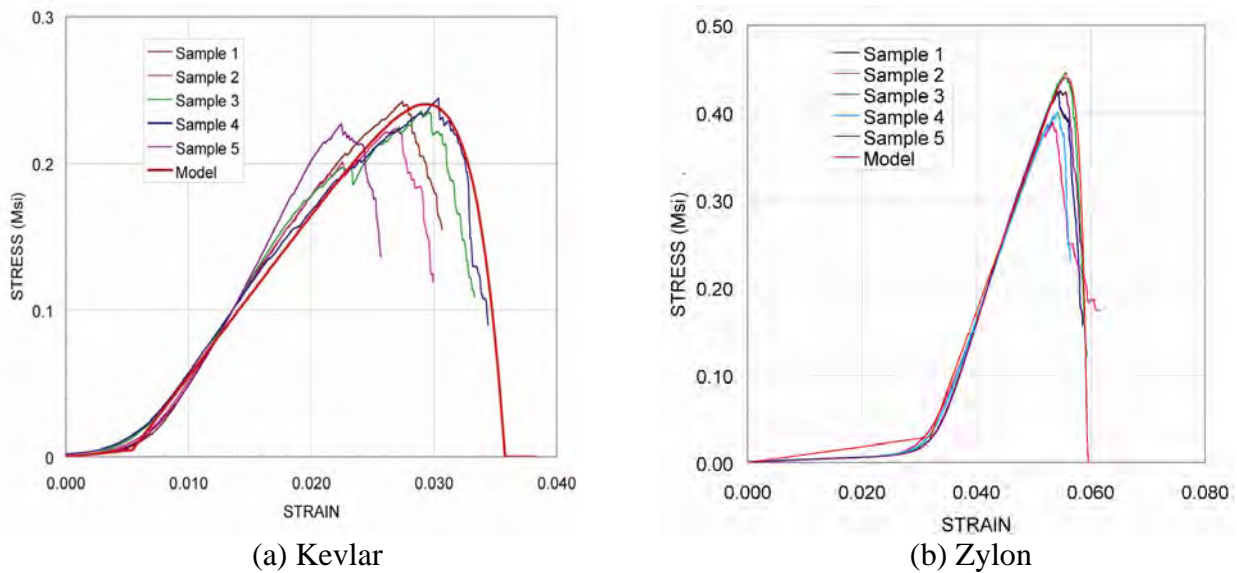


Figure 28. Uniaxial Tension Tests at ASU for Phase II and Version 3.1 Model Fit

3.2.2 Tensile Tests Over a Range of Strain Rates (Task 1.3.2).

Thirty-six fabric swath tensile tests were conducted at the UW Applied Biomechanics Laboratory in Seattle, WA, shown in figure 29. The tests involved 2 to 10 yarns of the three high-strength fabric materials: 500 D Zylon 35x35 fabric (Zy35), 1420 D Kevlar 49, 17x17 fabric (Kev17), and 1500 D Zylon 17x17 fabric (Zy17), at rates from quasi-static to nominally 250/s.



Figure 29. University of Washington Applied Biomechanics Laboratory

Figure 30 shows the test setup. A high-rate MTS testing machine, with ram displacement rates of up to 12 m/s (475 in./s), recorded load and ram displacement, while a Vision Research

The test specimens were constructed from 1-in.-wide swaths of the three different fabric materials received from Lincoln Fabrics of Ontario, Canada. Yarns from either side of the specimen were cut, leaving 2 to 10 yarns to resist the load. A failed specimen is shown in figure 32. Good results were obtained for tests up to about 25/s, but mechanical ringing in the load cell-to-specimen grip structure interfered with data at higher strain rates. The load cell with the grip connected could not respond fast enough to measure the load in the fabric for rates at or above 25/s. Thus, results are only reported for rates of 10/s and below.

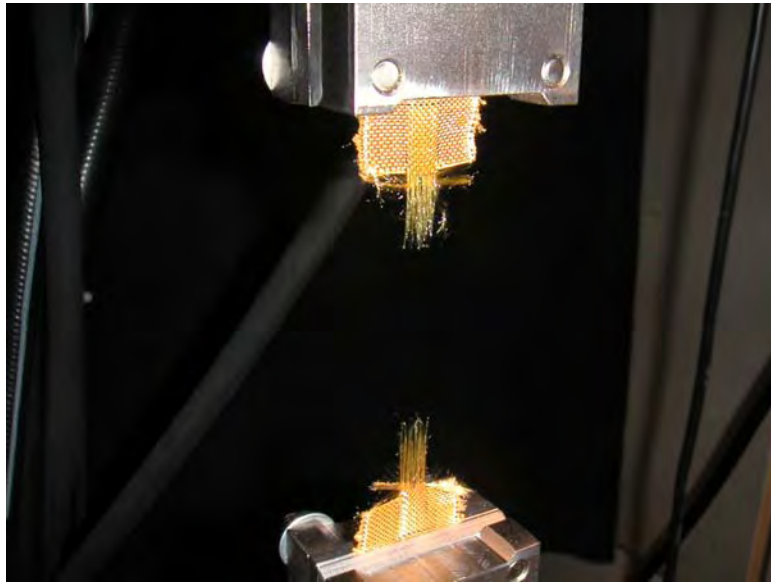


Figure 32. Failed Specimen

3.2.3 Zylon Strain Dependence Rate Tests.

Results from the strain rate dependence Zy35 swath tensile tests are shown in figure 33. The strain rates shown, 0.01/s, 1.6/s, and 13/s, (as well as the strains), are the actual values measured by the high-speed camera, and are lower than the strain rates calculated from the ram deflection (0.05, 4.6, and 28/s, respectively) due to slip at the grips. The slight oscillations on the rise for the highest-rate test shows the start of a mechanical resonance that was observed at this rate, and which becomes dominant at higher rates. The stepped structure on the fall of the slowest-rate test are the result of yarns (or groups of yarns) failing at staggered times (which is clearly visible on the camera records.) The results show a negligible strain-rate effect on tensile modulus, but a definite effect on tensile strength. Also included for comparison are previous quasi-static swath tensile test results and the Version 1.0-Z1A stress-strain model.

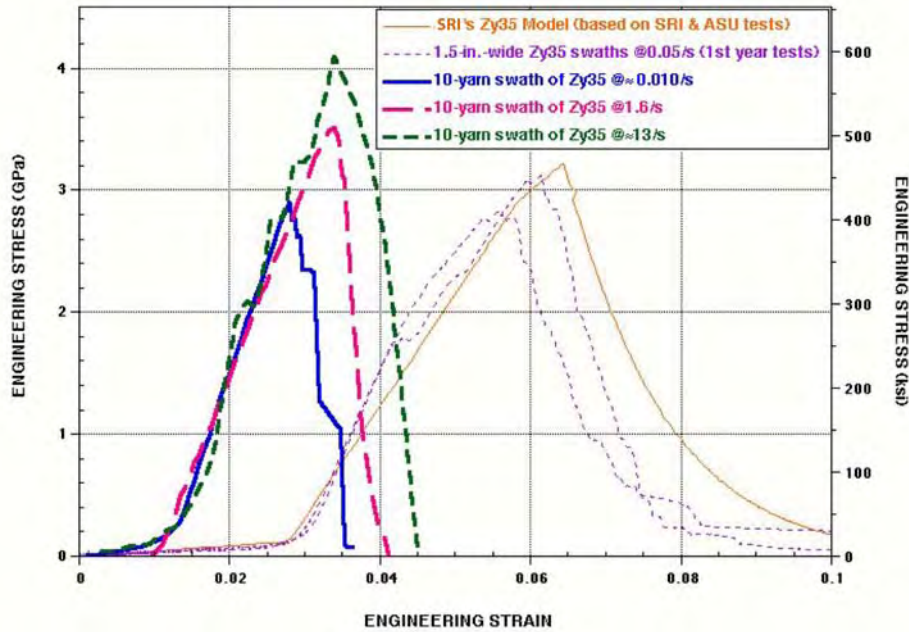


Figure 33. Variable-Rate Zylon Tensile Test Results

3.2.4 Kevlar Strain Rate Dependence Tests.

Results for the high-rate Kev17 swath tensile tests are shown in figure 34. The strain rates are 0.007/s, 1.3/s, and 12.5/s, respectively. The strain-rate effect upon tensile strength does not appear as strong as for Zy35. As with the Zy35, there appears to be negligible strain-rate effect upon tensile modulus.

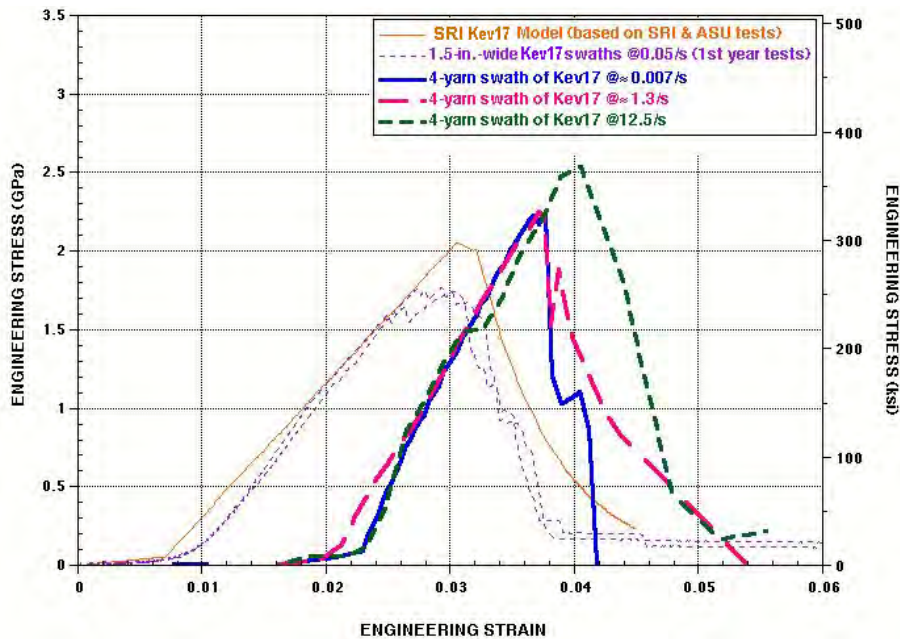


Figure 34. Variable-Rate Kevlar Tensile Test Results

3.2.5 Combined Strain Rate Test Results.

Combined data for the variable-rate Kevlar and Zylon tests in terms of normalized strength as a function of strain rate are shown in figure 35. At the maximum rate tested, about 10/s, Kevlar strength increased approximately 15% and Zylon strength increased approximately 40%.

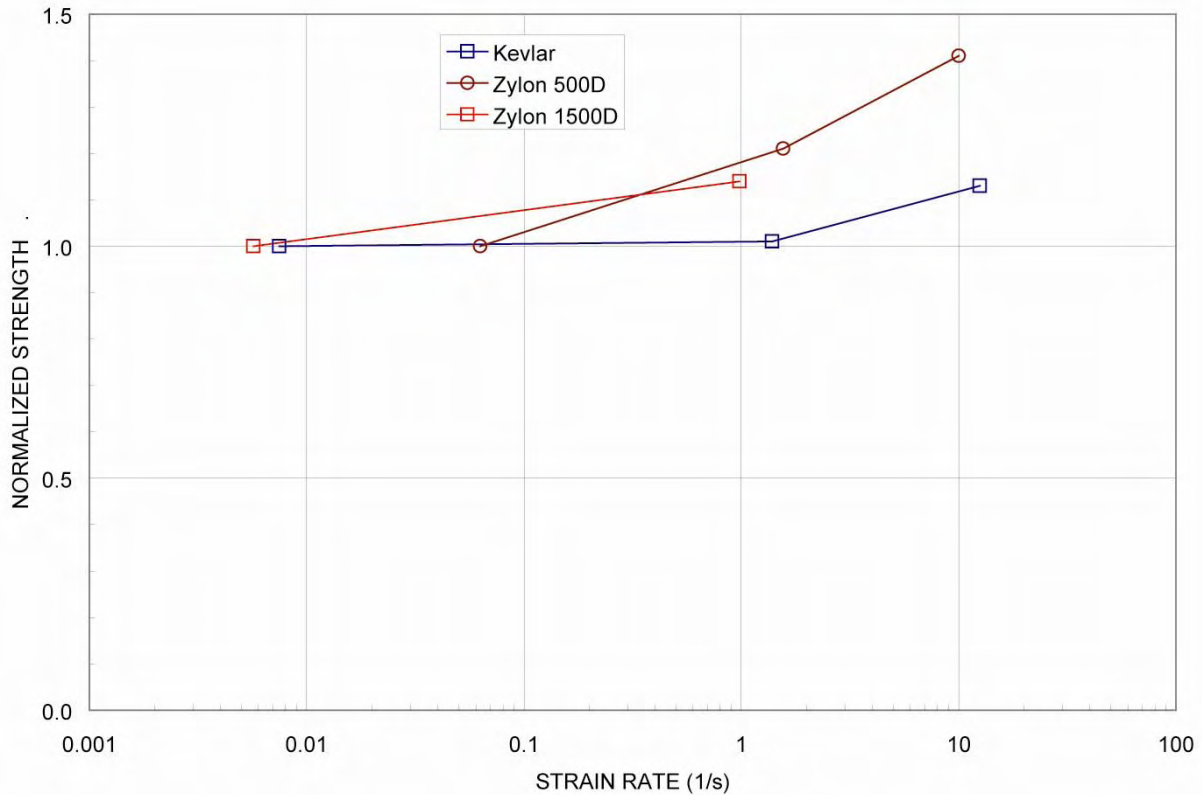


Figure 35. Rate Test Strength Summary

3.3 STATIC RING TEST-TO-FE RESULTS COMPARISON (TASK 1.6).

Comparison of the model to the results of the off-design static ring tests performed at ASU gives important information about structural modeling because the geometry of the interaction is correct between the projectile and fabric. The quasi-static ring test includes the penetrator contacting and deforming the fabric that is supported in a ring geometry, and includes the fabric draping the penetrator as it displaces the fabric. (See Part 1 (ASU) of this four-part report for more test details.)

The key to these simulations is to obtain values for the fabric failure for different projectile orientations. The simulations were performed without allowing the fabric to fail, and the stress values in the fabric were recorded at the test displacement when the failure first occurred. By comparing these stress failure values to those found in the tension tests, the effect of geometric and numerical conditions on the values for failure strength were assessed, as described in the following sections.

3.3.1 Simulation of 0° Ring Test With Constants From Static Uniaxial Test.

Results of a simulation of the 4-ply Kevlar 0° ring test conducted by ASU in Phase I of this program are shown in figure 36. Note that for these data, the ring test results have been shifted along the x-axis to match the location of increased stiffness for the test and model.

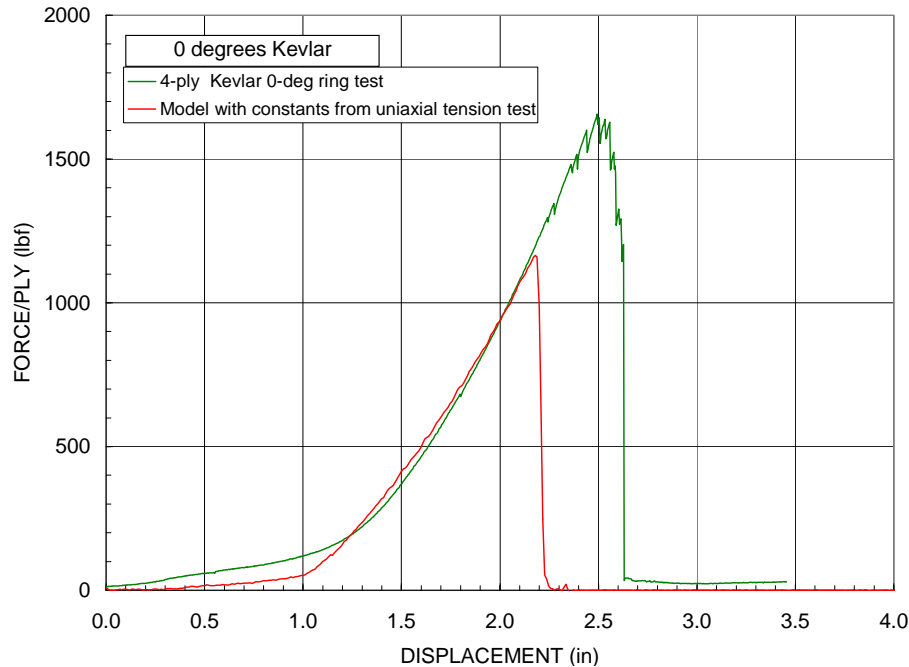


Figure 36. Simulation of 4-Ply Kevlar Ring Test With Constants K3A

A comparison of the simulation to the test results show that the Kevlar fabric model, with constants from the uniaxial tension tests, predicts a significantly lower strength and displacement to failure than the test results. The stresses in the fabric around the corners of the penetrator show stress concentrations that tend to fail the fabric early. This discrepancy between the test and model is most likely due to inaccurate modeling of the shear response of the fabric. Because the fabric is woven, it is very compliant in shear up to large shear deformations. Although a shear modulus was chosen that was small compared to the Young's modulus (the shear modulus is 5% of the Young's modulus), it was high enough to prevent the fabric from easily conforming to the around the corners of the penetrator. In choosing a value for shear modulus, choices were limited by the numerical stability of the model; i.e., if the shear modulus is too low, the element response can be unstable.

3.3.2 Adjustment to Failure Strength Based on Ring Test Results.

The strength parameters for the Kevlar were adjusted to better match the ring test data. The ring tests for the 0°, 45°, and 90° penetrators were rerun with the Kevlar fabric model, but with no failure allowed. The calculated force-displacement results are shown in figure 37.

Furthermore, unless some friction was included between the projectile and the fabric, the fabric would slip off the impactor before any damage to the fabric occurred. A coefficient of 0.2 was used for both static and dynamic friction in these simulations.

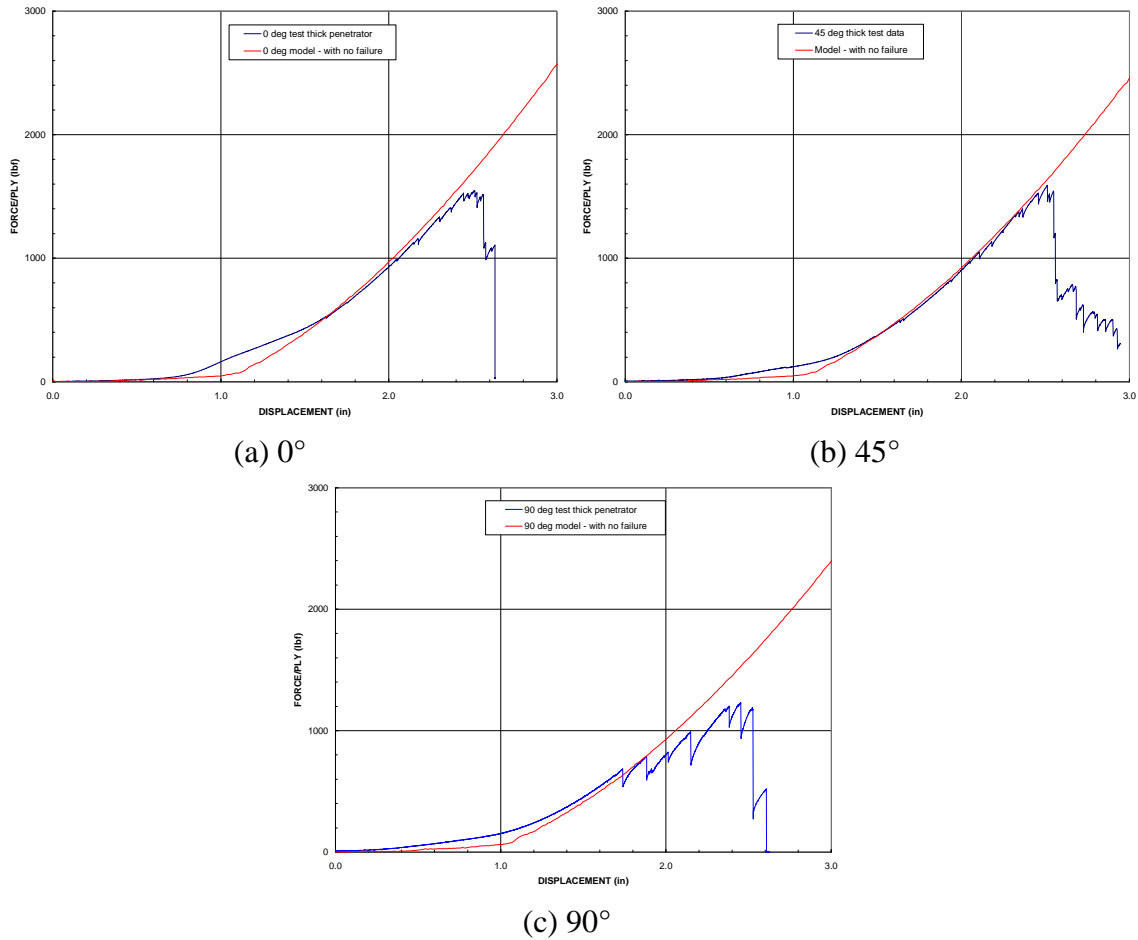


Figure 37. Ring Test Simulations Without Allowing Failure

Based on the test results, the displacement at which the material failed in all three cases was approximately 2.6 in. To determine an appropriate value for failure stresses, the highest element stresses were tabulated at 2.6 in. displacement for the three ring test cases. In the Version 3 fabric model, the damage and failure of the fabric is caused by a combination of the stresses in the two yarn directions. The results are shown in figure 38.

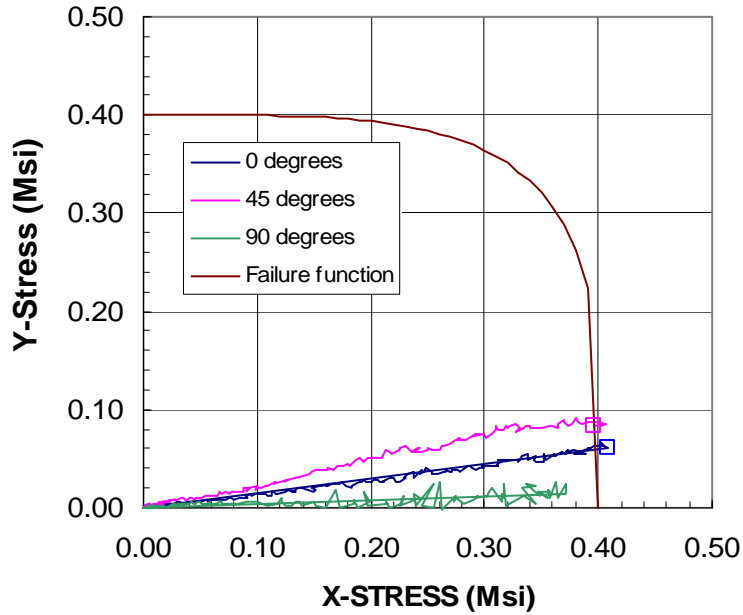


Figure 38. Failure Surface for Kevlar Fabric Based on Ring Test Results

The results of the ring tests suggested the strength of the fabric needed to be increased to better represent the peak stresses developed in the fabric ring during interaction with the penetrator. The modified constants set, K3B, has new values for ϵ_{\min} , ϵ_{\max} , σ_{\max} , and ϵ_{80} , as given in table 7.

3.3.3 Results of Ring Tests With Increased Strength.

Simulations of ring tests for 0° , 45° , and 90° orientation for both the thick and thin penetrator were performed using the constants set K3B. The results of the simulations are shown in figure 39. The difference between the results of the thick and thin penetrator for the simulations is small. For the 0° penetrator, the peak force for the thin penetrator is about 6% less than for the thick penetrator. This small difference was expected because the mesh size of the fabric elements (0.25 in.) was the same size as the thickness of the thick penetrator, and consequently, the fabric model did not have the resolution to distinguish between the thick and the thin penetrators ($3/16''$ thick).

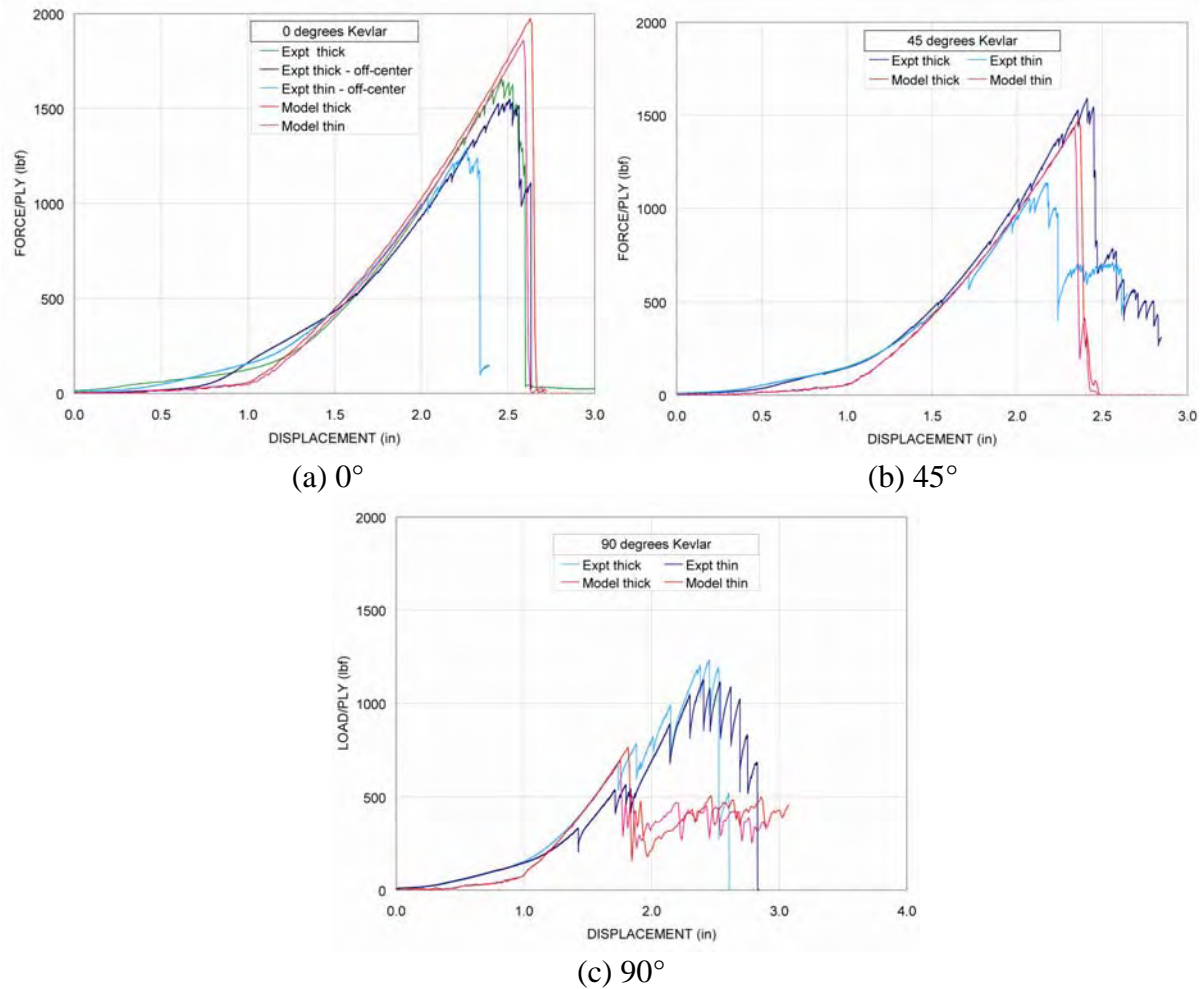


Figure 39. Kevlar Ring Test Simulation Results With Material Constant Set K3B

3.4 INITIAL FE SIMULATIONS OF NASA-GRC BALLISTIC TESTS (TASK 1.9).

3.4.1 Initial NASA-GRC Kevlar Simulations.

An initial set of simulations of the Kevlar NASA-GRC ballistic impact tests was performed by SRI, ASU, and Honeywell using Version 3.1 and the constants K3A as determined from the initial static uniaxial tests (listed in table 5) and using a time constant of 0.004 ms as determined from the previous phase of this program. As shown in table 10, the simulated ballistic tests included the old projectile, new projectile, 4, 8, and 32 plies, and a wide range of projectile orientations. The results of these simulations are also listed in table 10 and shown in figures 40 and 41. The model overpredicts the residual velocities for all the tests, in many cases, by a significant amount. That is, the fabric model was significantly weaker (absorbed less energy) than observed in the tests. Note that these simulations were performed with material set K3A before the strength constants were modified based on the ring test results described above.

Table 10. The NASA-GRC Ballistic Tests on Kevlar Targets With Model Version 3.1-K3A

Test No.	Penetrator Style	Fabric Plies	Impact Orientation			Impact V Test (ft/sec)	Residual V		Absorbed Energy	
			Pitch (deg)	Roll (deg)	Yaw (deg)		Test (ft/sec)	Model (ft/sec)	Test (%)	Model (%)
LG655	Old	32	1.3	-32.5	2.6	1131.7	830.6	1022.9	46.1	18.3
LG656	Old	32	-2.3	9.0	-10.1	967.3	469.2	832.9	76.5	25.9
LG657	Old	32	9.7	-22.2	1.4	829.7	0.0	705.5	100.0	27.7
LG688	Old	8	-20.5	10.5	62.8	870.9	549.3	634.5	60.2	46.9
LG689	Old	8	-1.3	-12.8	49.7	896.3	655.1	804.2	46.6	19.5
LG611	Old	8	-1.7	30.9	-10.8	905.7	798.1	848.9	22.4	12.1
LG612	Old	8	-3.7	22.8	-0.5	898.3	822.7	846.6	16.1	11.2
LG622	Old	8	-41.1	-50.7	72.5	872.7	625.7	809.0	48.6	14.1
LG624	Old	8	-2.9	-51.0	42.3	920.4	715.1	846.7	39.6	15.4
LG692	Old	8	2.3	38.2	41.5	885.3	602.6	794.9	53.7	19.4
LG594	New	8	6.6	27.0	47.8	843.9	484.5	697.5	67.0	31.7
LG609	New	8	0.9	37.4	1.6	913.7	825.4	889.6	18.4	5.2
LG610	New	8	0.7	25.3	11.9	888.1	809.7	836.7	16.9	11.2
LG618	New	8	6.3	-47.1	51.6	866.4	558.9	676.7	58.4	39.0
LG620	New	8	0.2	-37.8	55.1	893.8	580.8	735.0	57.8	32.4

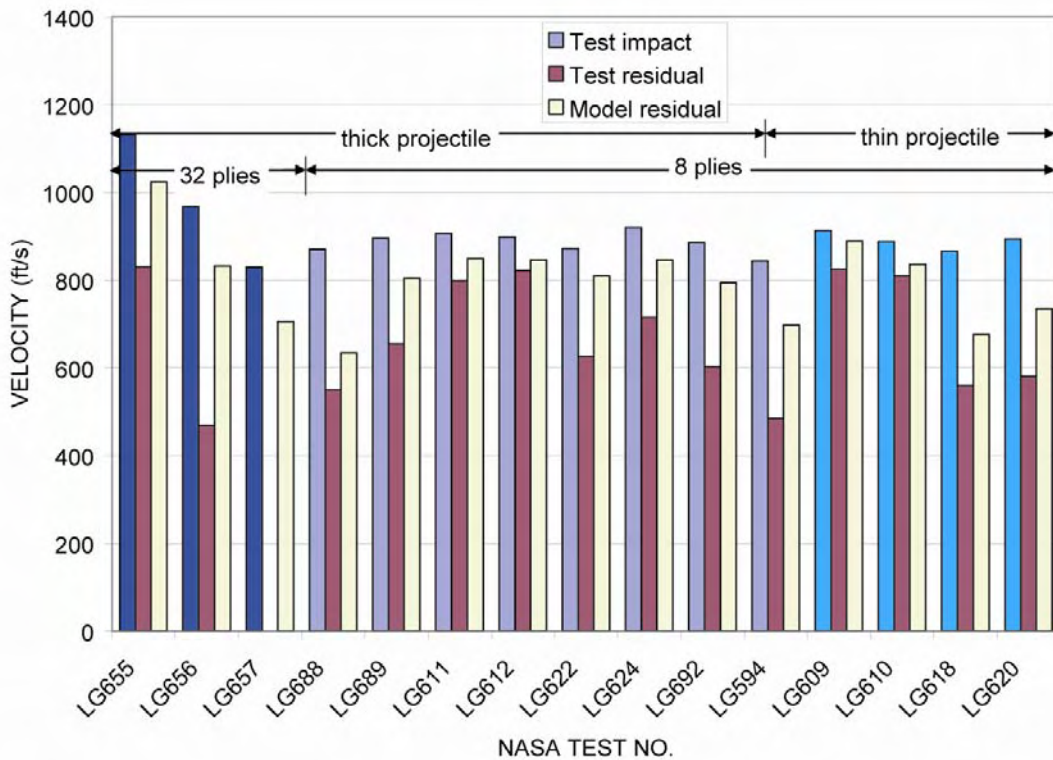


Figure 40. Version 3.1-K3A Simulations of NASA-GRC Kevlar Ballistic Tests

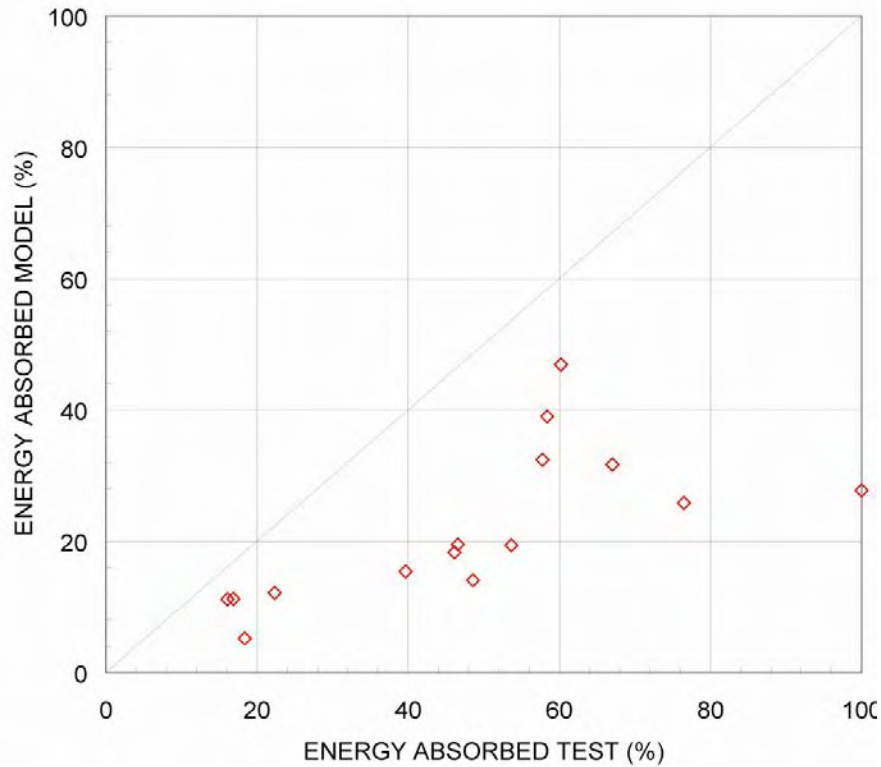


Figure 41. Energy Absorbed for Kevlar Tests Version 3.1-K3A

3.4.2 Initial NASA-GRC Zylon Simulations.

An initial set of simulations of the Zylon NASA-GRC ballistic impact tests was performed using Version 3.1 by SRI, ASU, and Honeywell using the constant set Z3A, as determined from the initial static uniaxial tests (listed in table 6) and using a time constant of 0.002 ms, as determined from previous phase of this program. As shown in table 11, the ballistic tests that were simulated included the old projectile, the new projectile, 8 and 32 plies, and a wide range of projectile orientations. (See Part 2 (NASA-GRC) of this report for more information on the projectiles.) The results of these simulations, including the residual velocity and energy absorbed, are also listed in table 11 and shown in figures 42 and 43. In general, the model underpredicted the residual velocity and overpredicted the energy absorbed for the tests that absorbed less than 20% of the impact kinetic energy; and the model overpredicted the velocity and underpredicted the energy absorbed for tests in which the energy absorbed was over 20%.

Table 11. The NASA-GRC Ballistic Tests on Zylon Targets With Model Version 3.1-Z3A

Test No.	Penetrator Style	Fabric Plies	Impact Orientation			Impact V Test (ft/sec)	Residual V		Absorbed Energy	
			Pitch (deg)	Roll (deg)	Yaw (deg)		Test (ft/sec)	Model (ft/sec)	Test (%)	Model (%)
LG658	Old	32	5.0	-9.0	0.4	1130.4	939.8	831.7	30.9	45.9
LG659	Old	32	2.1	6.8	5.3	1023.5	706.2	816.9	52.4	36.3
LG660	Old	32	-9.0	-5.0	-0.2	967.7	549.2	811.0	67.8	29.7
LG690	Old	8	-13.3	-24.5	39.3	895.7	654.2	759.7	46.6	28.1
LG626	Old	8	-5.2	25.1	-6.3	901.4	786.1	793.5	23.9	22.6
LG627	Old	8	-8.5	33.2	-10.4	816.0	650.2	709.3	36.5	24.4
LG639	Old	8	-7.4	61.3	9.2	934.6	809.8	874.8	24.9	12.3
LG694	Old	8	2.0	80.6	52.9	900.3	560.4	801.0	61.3	20.1
LG695	Old	8	-0.7	37.0	50.0	905.9	569.9	814.1	60.4	19.0
LG644	Old	8	-3.8	88.2	-1.9	910.7	842.9	832.5	14.3	16.4
LG645	Old	8	-1.9	68.8	0.5	917.3	824.8	818.1	19.1	20.5
LG646	Old	8	1.5	2.3	-5.8	915.3	842.3	806.7	15.3	22.1
LG647	Old	8	-4.3	24.5	-1.9	929.8	923.0	807.0	1.5	24.5
LG640	New	8	0.1	-6.4	-2.7	885.3	829.8	816.7	12.2	14.9
LG641	New	8	7.0	2.7	7.8	892.3	835.7	831.7	12.3	13.1
LG642	New	8	1.4	44.3	1.0	904.9	849.2	834.2	11.9	15.0
LG643	New	8	-4.7	44.9	-1.2	894.2	779.2	820.8	24.1	15.7

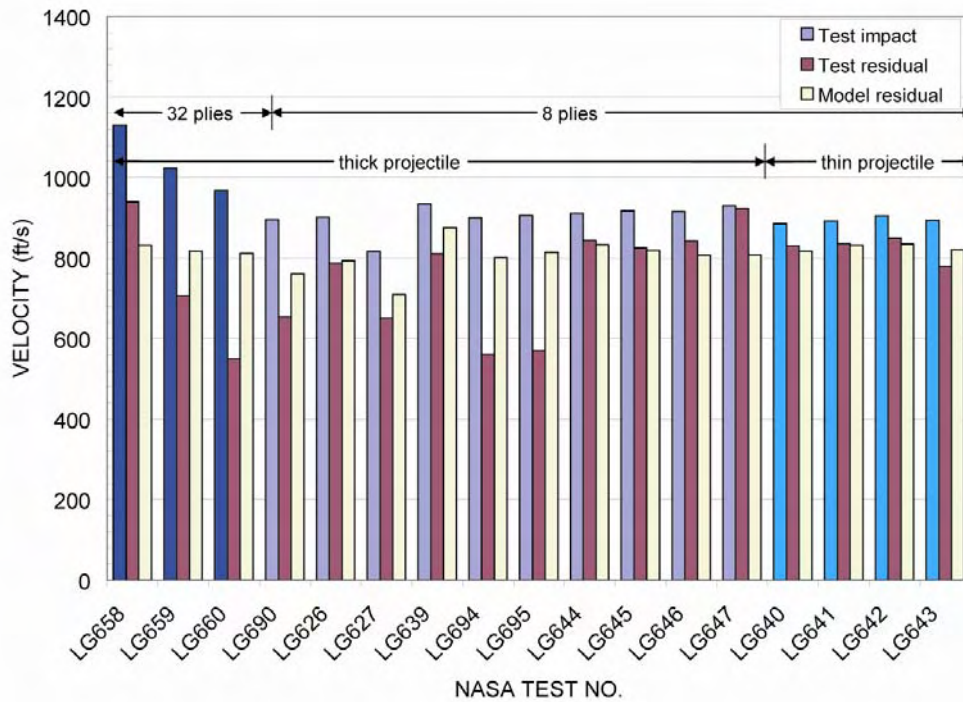


Figure 42. Version 3.1-Z3A Simulations of NASA-GRC Zylon Ballistic Tests

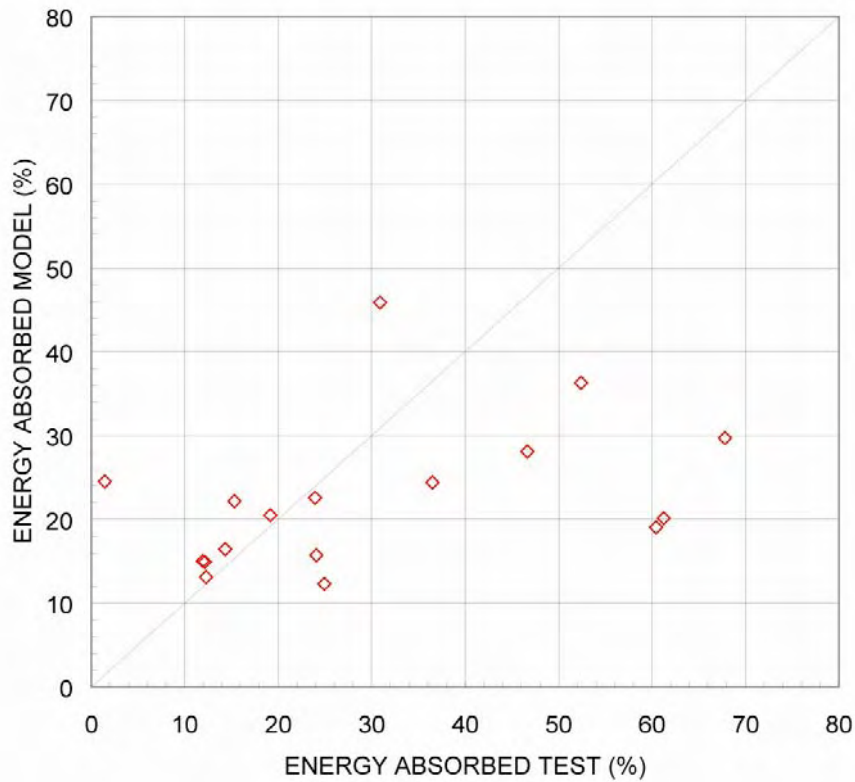


Figure 43. Comparison of Energy Absorbed for Zylon Model Version 3.1-Z3A

3.5 MATERIAL MODEL AND METHODS UPDATE (TASK 1.10).

3.5.1 Version 3.1-K3B Comparison With NASA-GRC Ballistic Tests.

A set of simulations was performed for the 18 NASA-GRC Kevlar ballistic impact tests listed in table 12 with the Version 3.1 of the ballistic fabric model using the material constants K3B listed in table 7. In addition to the tests simulated for the initial study (listed in table 10), four tests were added from Phase I. Note that in the Phase I tests, although the intended orientations were with zero pitch, roll, and yaw, the actual orientations were not measured during the test. For those test simulations, the pitch, roll, and yaw were assumed to be zero.

The results of the simulations for Version 3.1-K3B in terms of residual velocities are shown in figure 44. Of the 18 tests simulated, the calculated residual velocities for 10 tests were within 50 ft/s of the measured values; however, for three simulations, the calculated velocity was more than 100 ft/s greater than the measured velocity and for another three, the calculated velocity was more than 100 ft/s less than the measured velocity.

Table 12. The NASA-GRC Test Simulation Results for Kevlar Version 3.1-K3B

Test No.	Test Phase	Projectile Design	Mass (g)	No. Plies	Orientation			Velocity			Energy Absorbed	
					Pitch (deg)	Roll (deg)	Yaw (deg)	Impact (ft/sec)	Residual (ft/sec)	Model (ft/sec)	Test (%)	Model (%)
LG403	I	Old	318	4	N/A	N/A	N/A	894.0	845.0	855.1	10.7	8.5
LG404	I	Old	318	8	N/A	N/A	N/A	897.0	819.0	812.6	16.6	17.9
LG432	I	Old	320	16	N/A	N/A	N/A	896.0	650.0	688.8	47.4	40.9
LG411	I	Old	315	24	N/A	N/A	N/A	886.0	413.0	550.8	78.3	61.3
LG572	II	Old	320	2	21.0	0.0	13.0	346.6	295.0	291.5	27.6	29.3
LG611	II	Old	321	8	-1.7	30.9	-10.8	905.7	798.1	790.0	22.4	23.9
LG612	II	Old	321	8	-3.7	22.8	-0.5	898.3	822.7	786.6	16.1	23.3
LG688	II	Old	318	8	-20.5	10.5	62.8	870.9	549.3	600.3	60.2	52.5
LG689	II	Old	323	8	-1.3	-12.8	49.7	896.3	655.1	678.3	46.6	42.7
LG692	II	Old	316	8	2.3	38.2	41.5	885.3	602.6	722.8	53.7	33.3
LG655	II	Old	313	32	1.3	-32.5	2.6	1131.7	830.6	782.3	46.1	52.2
LG656	II	Old	322	32	-2.3	9.0	-10.1	967.3	469.2	329.7	76.5	88.4
LG657	II	Old	325	32	9.7	-22.2	1.4	829.7	0.0	409.6	100.0	75.6
LG594	II	New	307	8	6.6	27.0	47.8	843.9	484.5	581.3	67.0	52.6
LG609	II	New	305	8	0.9	37.4	1.6	913.7	825.4	838.4	18.4	15.8
LG610	II	New	307	8	0.7	25.3	11.9	888.1	809.7	787.2	16.9	21.4
LG618	II	New	306	8	6.3	-47.1	51.6	866.4	558.9	0.0	58.4	100.0
LG620	II	New	316	8	0.2	-37.8	55.1	893.8	580.8	384.8	57.8	81.5

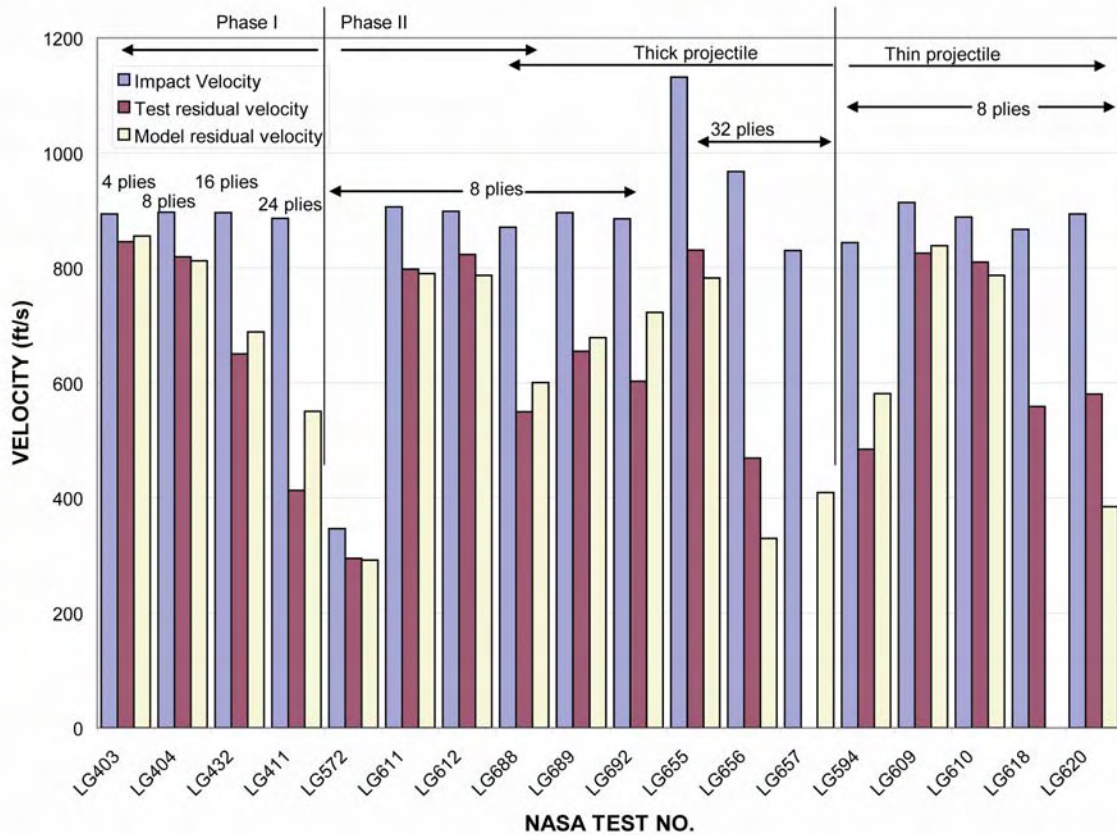


Figure 44. The NASA-GRC Ballistic Test Simulation Results for Kevlar for Version 3.1-K3B

Figure 45 shows the results of the simulations in terms of percentage of the initial KE absorbed. In these terms, in 11 of the 18 simulations, the calculated absorbed energy was within 10% of the measured values. The remaining seven simulations that were the furthest from the measured values were those in which the target absorbed a significant fraction of the initial KE.

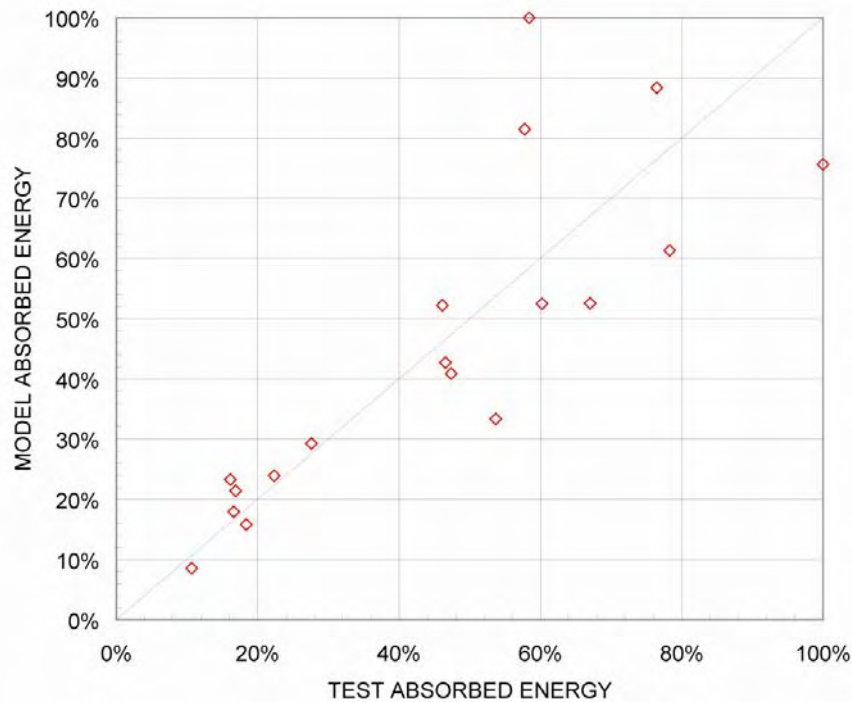


Figure 45. Percentage KE Absorbed for NASA-GRC Kevlar Test for Version 3.1-K3B

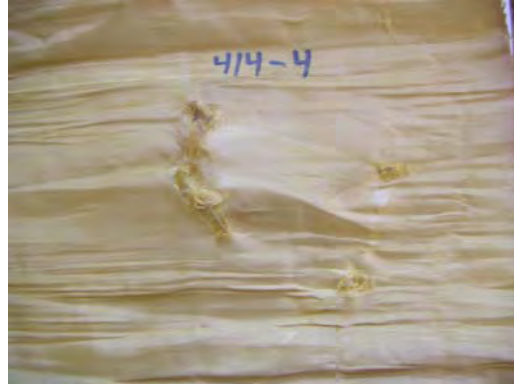
4. TASK 2: IMPROVE FE MODELING CAPABILITY FOR MULTIPLE LAYERS OF FABRIC.

4.1 REVIEW DAMAGE IN PARTIALLY PENETRATED FABRICS (TASK 2.1.1).

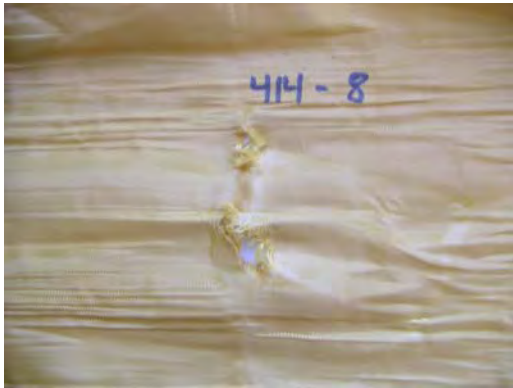
SRI received the posttest Zylon targets from NASA-GRC of the two Phase I tests in which the impactor was contained: LG407 and LG414. Both test specimens were 24 plies of Zylon. The damage pattern was the same for the two specimens: the inside plies failed first and sustained the most damage, the corners of the impactor caused the most damage, and the damage decreased as the outer layers were reached. The damage for successive plies for test LG414 is shown in figure 46. Ply 1, the inside ply, which was impacted first, shows the most damage, as seen in figure 46(a). The fabric has two large rips, one where the head of the impactor hit and a second below the initial impact point. There was other damage (apparently where the tail of the impactor hit after flipping), but it was limited to small holes at the corners of the impactor tail. Figure 46(b) shows the damage at ply 4, where the impactor head fully penetrated the fabric and there was damage at the corners of the tail. By ply 8, as shown in figure 46(c), the corners of the head had penetrated but the damage was not complete between those corners. The damage on ply 12, as shown in figure 46(d), was localized to the corners of the head. The damage on ply 16, as shown in figure 46(e), shows just dents in the fabric without penetration.



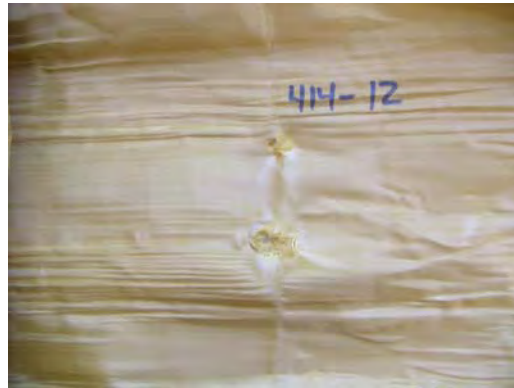
(a) Ply 1



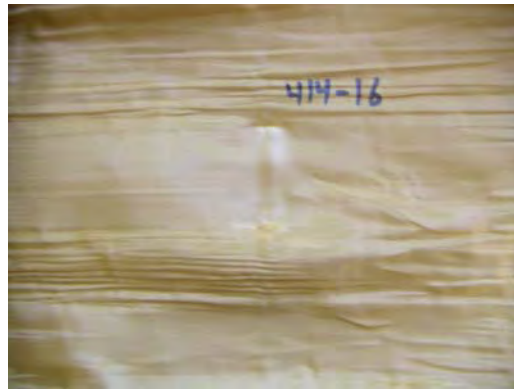
(b) Ply 4



(c) Ply 8



(d) Ply 12



(e) Ply 16

Figure 46. Ply Damage for Test LG414

4.2 REVIEW PROBLEM WITH LIVERMORE SOFTWARE TECHNOLOGY CORPORATION (TASK 2.2).

Based on previous simulations, mainly those by Honeywell, SRI found that multilayer simulations were often numerically unstable, meaning that either the simulation would crash and fail to complete, or that some result would be nonphysical; e.g., the calculated hourglass energy would be a significant fraction of the KE in the problem.

To help alleviate these problems, Fabio Montovani from Livermore Software Technology Corporation (LSTC) recommended investigating modifications to the analysis procedures used in this study that included changes to the hourglass formulation (use of viscous rather than stiffness hourglass control) or the use of element formulation 16 (rather than 2), which does not require hourglass control. LSTC also recommended adding a stiffness damping coefficient of 0.25. SRI performed 28 ballistic simulations to evaluate LSTC's recommendations. It was found that simulations with element type 16 were often unstable after penetration occurred, and that the use of stiffness damping in the fabric over a wide range of values for the stiffness coefficient had little influence on the results. Also, the choice of viscous or stiffness hourglass control had little influence on the stability of the simulations, although in some simulations, the choice of hourglass formulation can have an effect on the amount of energy absorbed.

After these investigations, SRI recommend the following guidelines for using multiple shell layers:

1. Use the contact formulation for *CONTACT_ERODING_SINGLE_SURFACE, which is the simplest method for defining the potential contact surfaces and includes element erosion.
2. Use the alternative contact formulation (SOFT=2).
3. Include the allowance for eroding contact (erosop=1).
4. Include the check for edge-to-edge penetrations (edge=2).
5. For the other parameters, as much as possible, use the default values.

4.3 MATERIAL MODEL AND METHODS UPDATE (TASK 2.4).

To test the effect of modeling with multiple layers of shell elements, SRI performed simulations for NASA-GRC tests LG646 and LG647, both 8-ply Zylon tests using Version 3.1-Z1A. As shown in table 11, the two test conditions were close to each other, the impact velocities were within about 2% of each other (915.2 and 929.8 ft/s), there was little pitch or yaw in either case, and only the roll angle (24.5° for LG647 compared to 2.3° for LG646), which has not been shown to have a large effect on energy absorbed, was different. However, there was a large difference in the fabric response for the two tests. Test LG646 absorbed 1.43 kft-lb of KE (15.3% of the impactor KE), but test LG647 absorbed only 0.14 kft-lb (0.15% of the impact KE), i.e., only about 10% of the energy absorbed in LG646.

For modeling with multiple layers of shell elements, two arrangements of shell elements were considered based on the different values for the shell element thickness listed in table 4, and the four measured fabric layers listed in table 3. In the first method, shell elements were spaced at a distance equal to the element thickness so that the inner and outer surfaces of adjacent elements just touched, i.e., a tight arrangement of elements. In the second method, the element spacing was based on the physical thickness of the fabric layers, thus resulting in a loose arrangement of elements. For all the simulations reported here, the tight arrangement of elements was used.

Simulations were performed for LG646 and LG647 for two configurations each: first with a single layer of shell elements representing 8 plies of Zylon, and a second configuration with two layers of shell elements, each layer representing 4 fabric plies. In coordination with LSTC, the contact parameters were chosen as listed in table 13. Eroding single-surface contact was used with SOFT=2, and the only nondefault parameter values were static and dynamic friction coefficients, FS and FD, of 0.2 (based on the ring test results), allowance for eroding contact (EROSOP=1), scale factor on the contact stiffness, SOFSCL, of 0.2 (default is 0.1), and a check to include edge-to-edge penetrations (EDGE=2).

Table 13. Contact Parameters for Multilayer Shells

*CONTACT_ERODING_SINGLE_SURFACE							
\$ SSID	MSID	SSTYPE	MSTYPE	SBOXID	MBOXID	SPR	MPR
0	0	5	0				
\$ FS	FD	DC	VC	VDC	PENCHK	BT	DT
0.2	0.2						
\$ SFS	SFM	SST	MST	SFST	SFMT	FSF	VSF
\$ ISYM	EROSOP	IADJ					
0	1						
\$ SOFT	SOFSCL	LCIDAB	MAXPAR	EDGE	DEPTH	BSORT	FRCFRQ
2	0.02			2		10	
*END							

The calculated velocity histories for the four simulations are shown in figure 47. The time response in all cases was very similar; the impactor penetrated the fabric and reached a steady state velocity at between 0.40 and 0.45 ms. In both cases, the simulation with multiple layers ended up with slightly higher velocity than the simulation with a single layer.

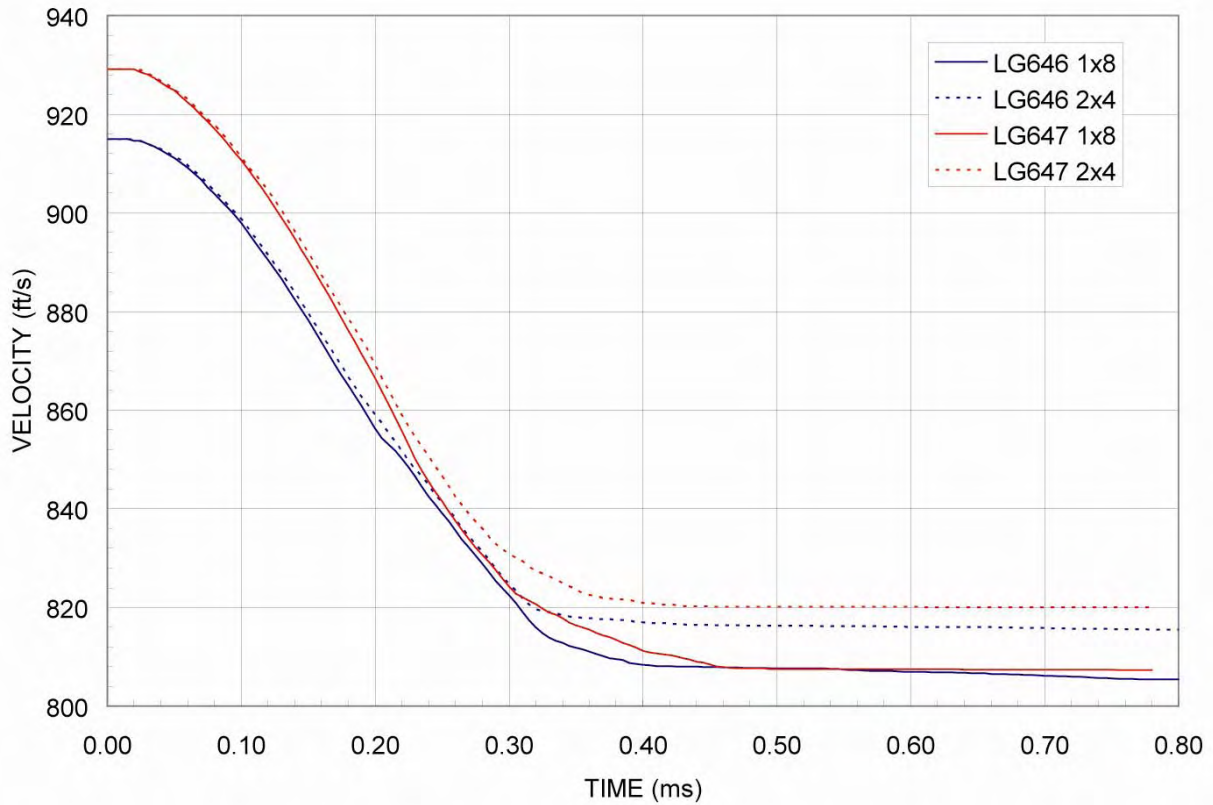


Figure 47. Effect of Modeling With Multiple Layers

The results for residual velocity and energy absorption are shown in table 14 and plotted in figure 48. In the simulations, the results for velocities and energy absorbed for the two tests were very similar to each other, unlike the test results described above. In both cases, the simulations absorbed more energy than the tests, and there was little difference between the calculated energy absorbed by a single shell layer and the energy absorbed by two layers of shells (within 1.5% for LG646 and 10% for LG647). These simulations show that, at least for a limited number of shell layers, multiples plies of fabric can be modeled with multiple shell layers.

Table 14. Results of Multiple Shell Simulations of LG646 and LG647

NASA Test No.	Result Type	Mass (g)	Before Impact		After Impact		Absorbed Energy	
			Velocity (ft/sec)	Energy (kft-lb)	Velocity (ft/sec)	Energy (kft-lb)	(kft-lb)	(%)
LG646	Test	326.4	915.3	9.35	842.3	7.92	1.43	15.3
	Model 1x8	315.1	915.0	9.02	805.4	6.99	2.03	22.5
	Model 2x4	315.1	915.0	9.02	807.3	7.02	2.00	22.2
LG647	Test	322.7	929.8	9.54	923.0	9.40	0.14	1.5
	Model 1x8	315.1	930.0	9.32	807.3	7.02	2.30	24.6
	Model 2x4	315.1	930.2	9.33	820.0	7.25	2.07	22.3

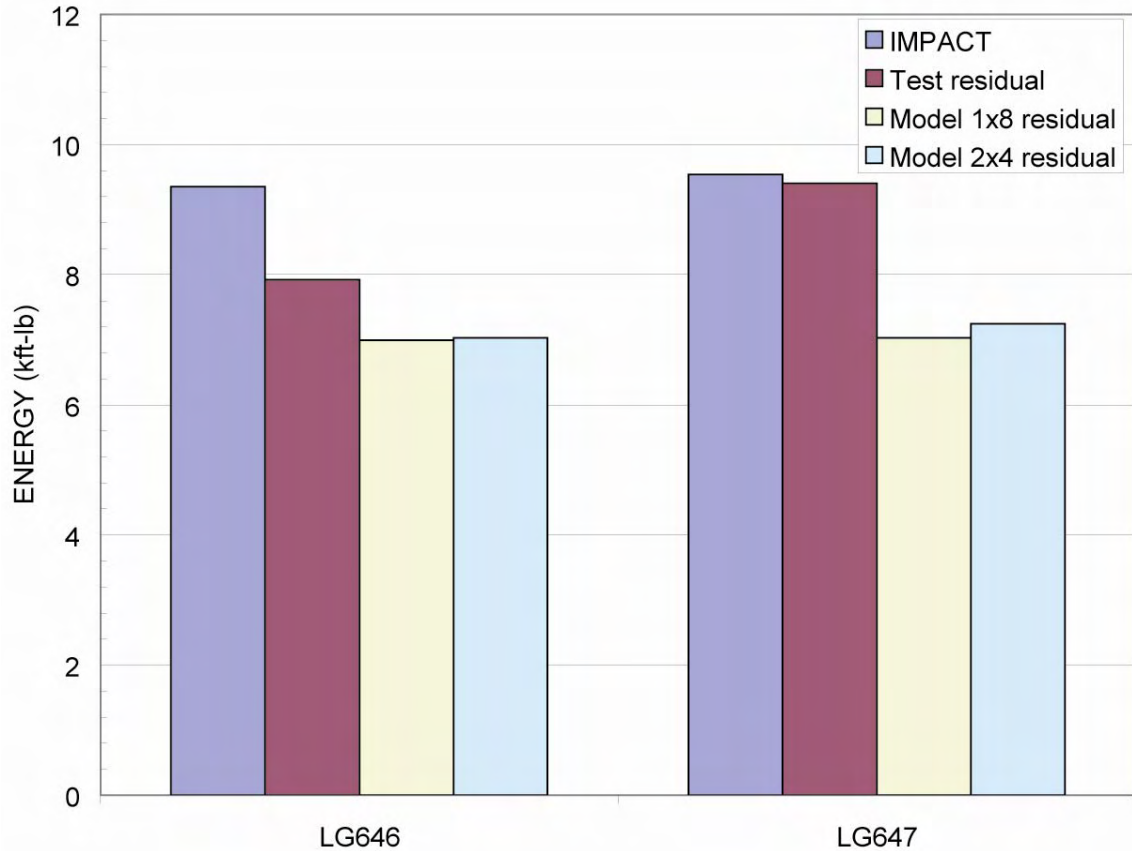


Figure 48. Kinetic Energy for Multilayer Simulations

4.4 DEMONSTRATE RESULTS: MULTIPLE SHELL LAYER SIMULATIONS FOR NASA-GRC KEVLAR TESTS (TASK 2.3).

SRI simulated the 16 NASA-GRC Kevlar tests listed in table 10 using multiple shell layers and Version 3.1-K3B. Four fabric plies were chosen for each shell layer that would give good resolution to distinguish damage, yet still be practical to run on existing SRI computers.

Table 15 shows the results of the simulations in terms of the calculated residual velocities for the single and multiple layers cases compared to the test values and the difference in KE absorbed between the single and multiple layer cases normalized by the impact KE. Comparing the difference in KE absorbed between the single and multiple layers, of the 16 cases, 11 were within 5% of each other, 1 was between 5% and 10%, 2 were between 10% and 20%, and 2 were between 20% and 50%.

For all the cases in which the difference was greater than 5%, the single shell layer absorbed more energy than the multiple shell layer; i.e., the multiple shell layers failed earlier. Compared to the test results, the multiple layers absorbed less energy than the test; but for the single layer simulations, the results were inconsistent; i.e., some absorbed more energy than the test, and some absorbed less energy than the test.

Table 15. Multiple Shell Layer Results Version 3.1-K3B

Test No.	Plies	Velocity				KE	
		Test Impact (ft/sec)	Test Residual (ft/sec)	Model Single Shell (ft/sec)	Model Multishell (ft/sec)	Absorbed Test (%)	Difference/ Impact (Single-Multiple) (%)
LG404	8	897.0	819.0	812.6	808.9	16.6	-0.7
LG611	8	905.7	798.1	790.0	793.8	22.4	0.7
LG612	8	898.3	822.7	786.6	785.3	16.1	-0.3
LG688	8	870.9	549.3	600.3	589.6	60.2	-1.7
LG689	8	896.3	655.1	678.3	664.9	46.6	-2.2
LG692	8	885.3	602.6	722.8	700.4	53.7	-4.1
LG594	8	843.9	484.5	581.3	583.5	67.0	0.4
LG609	8	913.7	825.4	838.4	842.0	18.4	0.7
LG610	8	888.1	809.7	787.2	785.0	16.9	-0.4
LG618	8	866.4	558.9	0.0	595.7	58.4	47.3
LG620	8	893.8	580.8	384.8	577.5	57.8	23.2
LG432	16	896.0	650.0	688.8	675.5	47.4	-2.3
LG411	24	886.0	413.0	550.8	528.9	78.3	-3.0
LG655	32	1131.7	830.6	782.3	838.8	46.1	7.2
LG656	32	967.3	469.2	329.7	537.1	76.5	19.2
LG657	32	829.7	0.0	409.6	497.3	100.0	11.6

Figure 49 shows the kinetic energy of the impactor for the tests and simulations. For the most part, the single and multiple shell simulations show good agreement with each other especially for the cases that do not lose much energy. The notable exceptions are the two 32-ply tests (LG656 and LG657) and the two tests that used the thin projectile (LG618 and LG620) that lost the most energy.

Figure 50 shows the percentage KE absorbed for the single and multiple shell simulations as a function of the percentage of KE absorbed in the test. For tests in which up to 50% of the KE was absorbed, the multiple shell simulations closely match the single shell results, and both are close to the test results (within approximately 15% of the energy absorbed). For the cases that absorbed more than 50% of the KE, the results diverge. For the multiple layers, the simulations all absorbed less KE than the tests, but the single layer simulations were inconsistent; i.e, some absorbed more KE than the test, and some absorbed less.

The difference in percentage of absorbed KE for single and multiple layer simulations is shown in figure 51 as a function of the absorbed energy in the test. Most simulations are within 5% of each other, but for all the 32-layer simulations the difference was greater than 5%, as were 2 of the 8-ply tests. In all the cases with large differences, the test absorbed more than 50% of the KE.

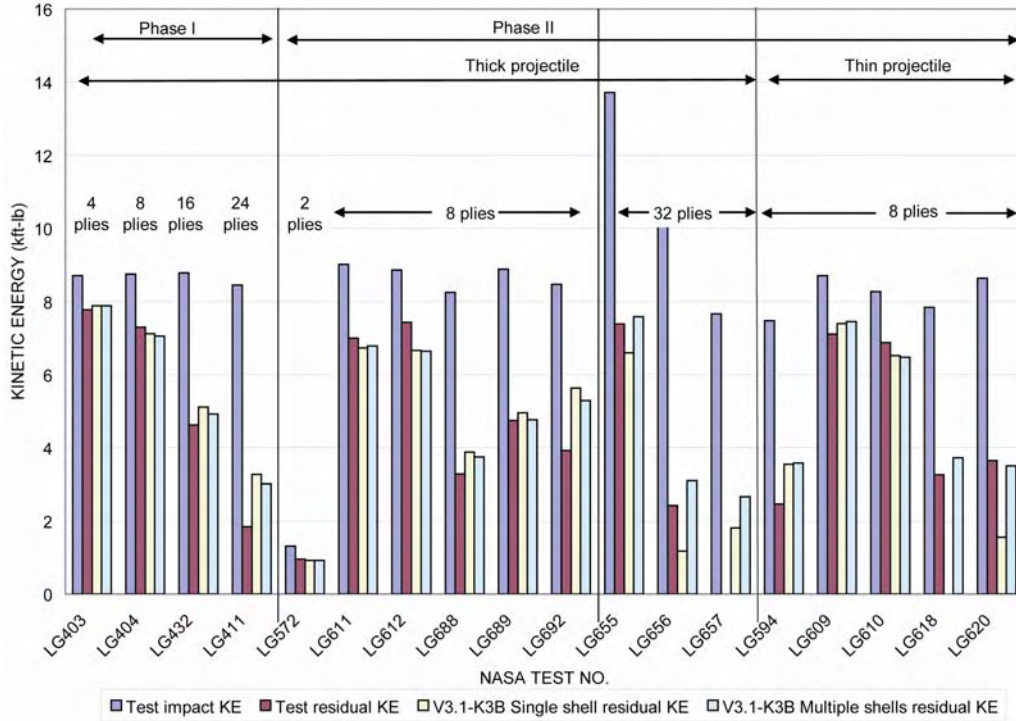


Figure 49. Kinetic Energy in Kevlar NASA-GRC Tests for Version 3.1-K3B Single and Multiple Shell Simulations

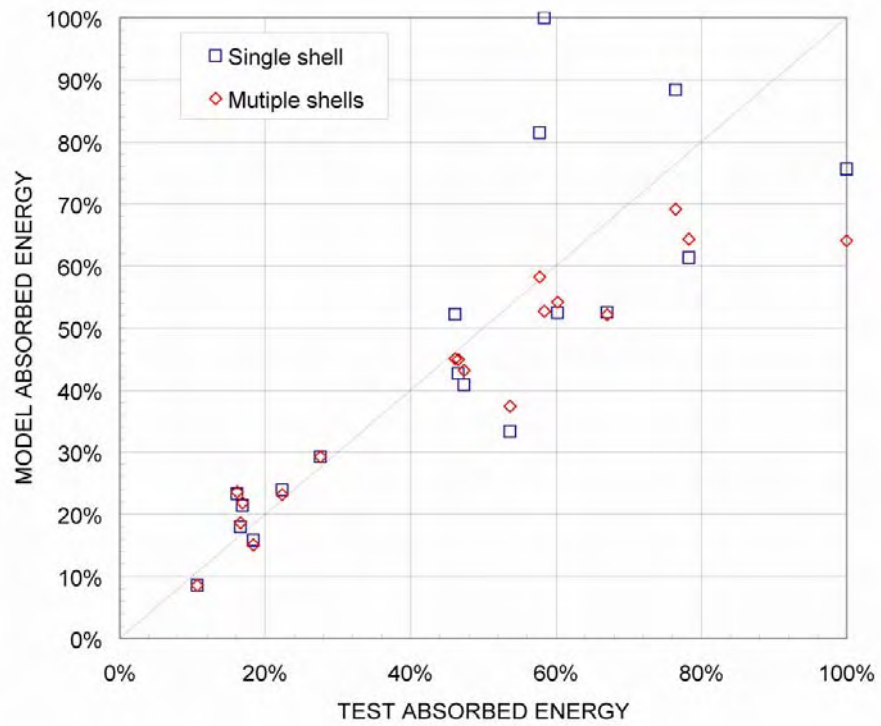


Figure 50. Energy Absorbed in NASA-GRC Kevlar Tests for Version 3.1 Multiple Layer Simulations

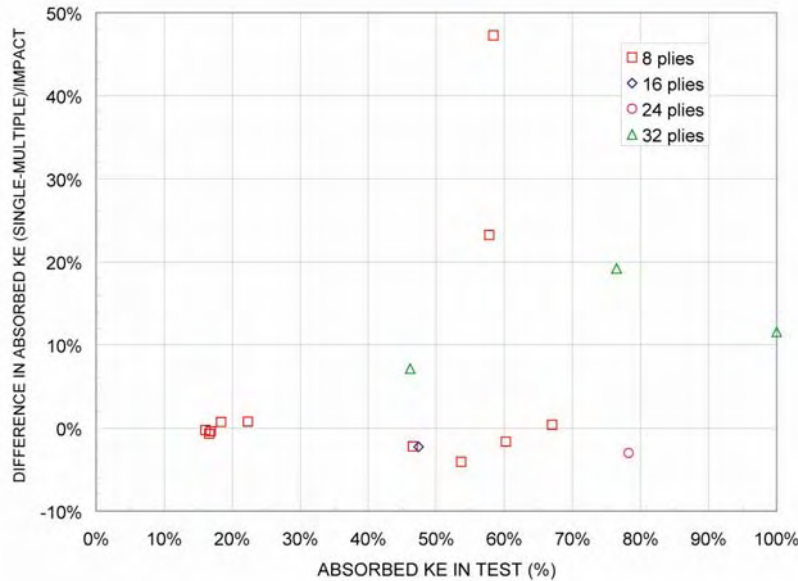


Figure 51. Difference in Absorbed KE for Single and Multiple Layer Simulations

5. CONCLUSIONS AND RECOMMENDATIONS.

5.1 CONCLUSIONS.

The conclusions from this research are as follows:

- A model parameter study was performed to identify the important material parameters in the model. The parameters with the most significant effect on the response were tensile modulus, shear modulus, strength, failure strain, and rate dependence. The effect of these parameters on stress and energy absorbed can be very nonlinear.
- Tensile tests at high rate showed a significant increase in strength with rate, but the highest rates successfully tested (about 10/s) were still below those of interest (up to about 400/s).
- Using material constants from uniaxial stress tests on Kevlar[®] (constants set K3A) to simulate the static ring tests, underpredicted the strength, especially for the 90° ring test. The simulations were improved by increasing the strength of the Kevlar (constants set K3B) based on estimating the stresses based on the value of penetrator displacement in the tests.
- For Kevlar, Version 3.1 using material constants K3B for Kevlar and a single element layer to model the fabric showed reasonable agreement over a wide range of projectile orientations and a number of fabric layers. In terms of percentage of kinetic energy (KE) absorbed, in 11 of the 18 simulations, the calculated absorbed energy was within 10% of the measured values. The simulations that were the furthest from the measured values were those in which the target absorbed a significant fraction of the initial KE.

- For Zylon[®], Version 3.1-Z3A underpredicted the residual velocity and overpredicted the energy absorbed for the tests that absorbed less than 20% of the impact KE, which the model overpredicted the velocity and underpredicted the energy absorbed for tests in which the energy absorbed was over 20%.
- The multiple shell simulations closely matched the single shell results for tests in which up to 50% of the KE was absorbed, and both are close to the test results (within about 15% of the energy absorbed). For the cases that absorbed more than 50% of the KE, the results diverge from each other. For the multiple layers, the simulations all absorbed less KE than the tests, but the single layer simulations were inconsistent, some absorbed more KE than the test and some absorbed less. More investigation is necessary to explain these results.

5.2 RECOMMENDATIONS.

As a result of this research, the following tasks are recommended for future research:

- The test results from National Aeronautics and Space Administration Glenn Research Center (NASA-GRC), mainly the videos, need to be better analyzed and understood. Initial attempts at correlating projectile orientation and energy absorbed were unsuccessful. Furthermore, some tests that appeared to have nearly the same impact conditions absorbed significantly different amounts of energy. To implement the actual energy absorbing mechanisms into the model, the actual response needs to be better understood.
- Along with studying the videos of the tests for insight, the simulations need to be compared more closely with high-speed videos. The simulations that absorbed either significantly more or less energy than the test would be of most interest. The simulations that gave the least accurate results tended to be those that absorbed a large fraction of the energy. In those cases, other mechanisms such as friction between the fabric and projectile or yarns that hung onto the projectile without failing may have made a difference in the fabric response.
- The damage and failure algorithm for the model needs to be further developed. Specifically, the response of the fabric when the projectile is oriented at 90° to the loaded yarns needs improvement. Also, there is a need to look at methods that allow the fabric to resist ripping.
- More high-rate data needs to be collected for Kevlar and Zylon, particularly in the range of strain rates from 10-500/s.

6. REFERENCES.

1. Rajan, S.D., Mobasher, B., Sharda, J., Yanna, V., Deenadayla, C., Lau, D., and Dhah, D., “Explicit Finite Element Modeling of Multilayer Composite Fabric for Gas Turbine Engines Containment System, Part 1: Static Tests and Modeling,” FAA report DOT/FAA/AR-04/40,P1, November 2004.
2. Periera, M. and Revlock, D., “Explicit Finite Element Modeling of Multilayer Composite Fabric for Gas Turbine Engines Containment System, Part 2: Ballistic Impact Testing,” FAA report DOT/FAA/AR-04/40,P2, November 2004.
3. Simons, J., Erlich, D., and Shockey, D., “Explicit Finite Element Modeling of Multilayer Composite Fabric for Gas Turbine Engines Containment System, Part 3: Model Development and Simulation of Experiments,” FAA report DOT/FAA/AR-04/40,P3, November 2004.
4. Gomuc, R., “Explicit Finite Element Modeling of Multilayer Composite Fabric for Gas Turbine Engines Containment System, Part 4: Model Simulations for Ballistic Tests, Engine Fan-Out, and Generic Engine,” FAA report DOT/FAA/AR-04/40,P4, November 2004.